Erratum

Simulation and experimental study of texture in domains in lipid bilayers

Jonas Camillus Jeppesen
jojep07@student.sdu.dk

February 10, 2014

Note on this erratum

As is clearly evident from the work this erratum accompanies it was written in a very short period of time and hence contains quite a few typographical errors. This erratum will correct the most critical errors made in the unduly quick printing and writing process.

List of errors

Danish abstract (page 4)

A version control user error caused the wrong Danish abstract to be included in the final print. This is the correct one:

Lateral organisering af cellers plasmamembran har stor betydning for biologiske cellers funktion. In vivo studier af cellemembraner er meget vanskelige og studiet af understøttede modelmembraner er derfor et vigtigt første skridt mod at forstå processer i rigtige biologiske cellemembraner. I dette speciale projekt undersøges den laterale organisering af en modelmembran i det den gennemgår en $L_\alpha \rightarrow L_{\beta'}$ faseovergang fremtvunget ved nedkøling af membranen. Tidligere studier har vist, at lipid dobbeltlag, bestående af to forskellige lipider, danner faste gel-lignende domæner når de køles ned og at disse domæner udviser en orienteringstekstur i form af lipidernes tilt i forhold til menbranens normal. Kvalitative og kvantitative studier af form og tekstur af gel-domænerne eksisterer, men ingen af dem prøver at modellere hvordan de opstår i dobbeltlag. I dette projekt præsenteres en model som kvalitativt reproducere både tekstur og fysisk form af gel-domænerne. Modellen er baseret på en række eksisterende observationer og nye observationer lavet i forbindelse med dette projekt. Væksten af domænerne forstås som værende begrænset af diffusion i membranen og baseret på dette foreslås en diffusionsbegrænset vækst (DLA) model for domænernes vækst. Spørgsmålet om hvorvidt domænerne er termodynamisk i ligevægt og om de er stabile strukturer besvares. På korte tidsskalaer (timer) er de former der dannes under væksten stabile, men på længere tidskalaer (dage) er de ikke stabile; deres form afrundes og deres tekstur

bliver mere uniform. Spørgsmål til fremtidige eksperimentelle studier og simuleringer stilles også.

TODO-notes left in document (page 12)

page 12 (mid) The question of whether the *free energy* was energy minimized by the self-assembly process. This is indeed the correct "energy" pertaining to this phenomenon.

page 12 (mid) A discussion of the phenomenon that the phase transition can take place at different temperatures for the two bilayer leaflets[1] were intended to be included here.

page 20 (mid) Verification of the manufacturer of a silicone glue used in the experiments. The manufacturer stated is the correct one.

page 23 (top) A description of the laser used for Laser Scanning Microscopy was intended here. The laser used was a Spectra-Physics MaiTai Ti:sapphire laser (tunable, pulsed).

page 29 (mid) A question about scientific writing style was left here and the answer to it employed by the sentence "... to *my* knowledge ...".

Figures

Fig. 3 (page 8) The temperature axis on the figure is -20, 0, 20, -40 which is an error. It should be -20, 0, 20, 40.

Fig. 16 caption (page 33) The correlation function $C(r)$ at different times throughout the experiment.

Fig. 18 caption (page 34) Area and perimeter length for individual domains as a function of time.

Other errors

Eq. 5 (page 18) Missing mn superscript on I_k^{mn} in the sum: $\tilde{I}_\gamma^{mn} = \sum_{k=1}^{N} I_k^{mn} \cdot e^{-i2\pi\frac{1}{N}(\gamma-1)(k-1)}$

Eq. 6 (page 18) I_γ^{mn} should be I_3^{mn}: $\varphi_c^{mn} = -\frac{1}{2} \cdot R \cdot arg[I_3^{nm}] + \phi_o ffset$

Page 12 (top) The discussion of the lipid organization in dry films is valid for 100% dry lipid films, but in practice the membrane is always slightly hydrated due to moisture in the air. So what is called *dry films* in the thesis do indeed have their lipids organized as bilayers.

References

[1] D. Keller, N.B. Larsen, I.M. Møller, and O.G. Mouritsen. Decoupled phase transitions and grain-boundary melting in supported phospholipid bilayers. *Physical Review Letters*, 94(2):025701, 2005.

Master thesis

Simulation and experimental study of texture in domains in lipid bilayers

Jonas Camillus Jeppesen
jojep07@student.sdu.dk

Supervised by:
Associate professor Per Lyngs Hansen
Associate professor Adam Cohen Simonsen
Assistant professor Jonathan R. Brewer

6. februar 2014

Indhold

Abstract

Lateral organization of the cellular plasma membrane is of great importance because it plays a vital role in the function of biological cells. In vivo studies of cellular membranes are very difficult and the study of supported model membranes and important first step towards understand similar processes in real biological cell membranes. In this master thesis the lateral organization of lipids within the membrane is studied as it goes through an $L_\alpha \rightarrow L_{\beta'}$ phase transition induced by cooling of the membrane. Previous studies of this have found that lipid bilayer consisting of two different species of lipids exhibit formation of solid gel domains and that these gel domains contain orientational texture in form of the lipids tilting with respect to the membrane normal. Qualitative and quantitative studies of shape and texture of the gel domains exist, but none of them try to model how they come into being. In this thesis a model for the growth of the domains is presented which qualitatively reproduces both texture and shape of the domains. The model is based on a number of experimental observations made. The growth of the domains is recognized to be limited by diffusion in them membrane and based on that a diffusion limited aggregation model is proposed to model the growth of the domains. Experimentally it is also found that there is no coupling between englishthe texture and the shape of the domains. The question of whether the domains are stable structures in equilibrium is answered. On a time scale of hours the intrinsic shapes they form during growth is stable but on a time scale of days they are not stable and relax into more rounded shapes with more uniform texture. A number of interesting questions for future simulation studies are raised.

Resumé

Lateral orgnisering af den cellulÃęÃęre plasmamembranen er af stor betydning, fordi det spiller en afgÃÿrende rolle i funktionen af biologiske celler. In vivo studier af cellulÃęre membraner er meget vanskelig, og studiet af understÃÿttede modelmembraner og vigtigt fÃÿrste skridt i retning af at forstÃě lignende processer i reelle biologiske cellemembraner. I deette speciale den laterale organisering af lipider i membranen er undersÃÿgt, da det gÃěr gennem en $L_\alpha \rightarrow L_{\beta'}$ faseovergang fremkaldt ved afkÃÿling af membranen. tidligere undersÃÿgelser af dette har fundet, at lipid-dobbeltlag, der bestÃěr af to forskellige arter af lipider udviser dannelse af faste gel domÃęner, og at disse gel domÃęner indeholder orienteringshjÃęlp tekstur i form af lipiderne hÃęldende med hensyn til menbranen normalt. Kvalitative og kvantitative undersÃÿgelser af form og konsistens af gelen domÃęner eksisterer, men inagen af dem forsÃÿger at modellere , hvordan de kommer ind i vÃęsen. I denne afhandling er en model for vÃęksten af de domÃęner prÃęsenteres som kvalitativt gengiver bÃěde konsistens og form af domÃęner. Modellen er baseret pÃě en rÃękke eksperimentelle observationer. VÃęksten af domÃęnerne er kendt for at vÃęre begrÃęnset ved diffusion i dem membran og baseret pÃě, at en diffusion begrÃęnset sammenlÃęgning model foreslÃěet at modellere vÃęksten af domÃęner. Eksperimentelt er det ogsÃě konstateret at der ikke er nogen kobling mellem tekstur og formen af de domÃęner. SpÃÿrgsmolet om hvorvidt de domÃęner er stabile strukturer i ligevÃęgt er besvÃęaret. PÃě en tidsskala timer de iboende former der udgÃÿr under vÃęksten er stabil, men pÃě en tidsskala af dage, de ikke er stabile og slappe af i mere afrundede former med mere ensartet konsistens. En rÃękke interessante spÃÿrgsmÃěl til fremtidige simuleringsundersÃÿgelserne er rejest.

1 Introduction

In this thesis the thermodynamics of lipid bilayers are investigated. Lipid bilayers are of huge biological importance because they make up the walls of our cells. Lipid bilayers are self-assemblies of lipids. Lipids are long-chained organic molecules with a hydrophobic tail and a hydrophilic head. When immersed in water they self-assemble in a way which prevents the tails from coming into contact with the water. A bilayer is one such structure. In a bilayer the lipids are stacked on top of one another with the tails facing in towards the center of the bilayer and the heads facing out towards the water.

Like all other materials lipid bilayers exhibit phase transitions induced by changes in temperature. At low temperatures the lipids form a solid-like phase where the lipid tails become more stretched and rigid compared to higher temperatures. Patches of membrane in this solid-like state is called domains. When a domain is formed an unwanted situation arises because the lipids in the solid-like state are now longer than the lipids in the fluid-like state. The difference in height between the lipids int he two phases is called the hydrophobic mismatch because it exposes part of the hydrophobic chain of the lipids in the solid-like state to the surrounding water. To compensate for this the lipids in the solid-like phase can tilt with respect to the membrane normal. This effectively lowers the hydrophobic mismatch and is therefor energetically favorable over not tilting.

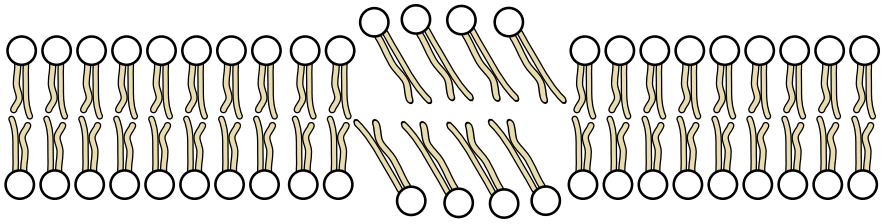

Figur 1: Lipid bilayer with a gel domain in the center. The tilted gel phase is shown which helps compensate for the hydrophobic mismatch between the lipids on solid form and the lipids on liquid form.

If such a domain is view from above it can be seen to have all shorts of shapes; from circular to flower-like. In different parts of the domain the lipids might tilt in different directions. If different directions of the tilt is given different colors the the domain might look like figure 2 when seen from above. The spatial distribution of the different angles of tilt called the texture. This project is concerned with the texture and shape of the domains and aims to answer the questions of why the domains are shaped like rosettes. The phenomenon was studied experimentally and using the experimental observations a computer model for the growth of the domains were made.

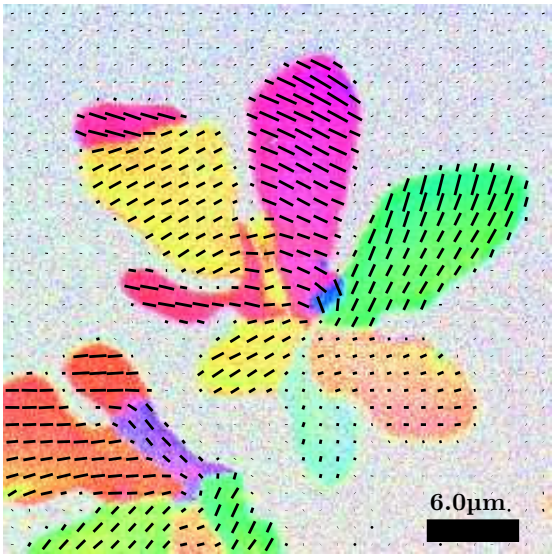

Figur 2: A domain seen from above displaying texture.

This very compact presentation of the work is structued as follows. First an short introduction to lipid bilayers and their phase behavior. Then the experimental techniques and data analysis will be covered followed by a presentation of the experimental results. The experimental results will be presented in the same sequence as the bilayers display them throughout their existence; beginning with the nucleation and initial growth and ending with the long-term behavior. After a summary of the experimental conclusions and findings the growth model will be presented based on the experimental findings. Discussion and conclusions will follow immediately after the relevant experimental results.

1.1 Phase transitions in bilayers of binary lipid mixtures

This is a short introduction to the phase behavior of binary lipid mixtures and is largely a short summary of what can be found in textbooks on the subject, for example [1, 2].

All experimental work in this thesis was done on bilayers of binary lipid mixtures. A binary lipid mixtures is a mixtures of two lipids. A self assembled lipid bilayer of such a mixture will, like most other materials, undergo phase transitions when the temperature of the bilayer is changed. At low temperatures the lipid tails will tend to be stretched, the area per lipid small and lateral movement of the lipids restricted. This phase is called the solid ordered phase, the gel phase, L_o or L_β. A mark is added to β if the lipids are tilted with respect to the bilayer normal. This phase will therefore be called $L_{\beta'}$ throughout this thesis. At higher temperatures the lipid tails tend to less stretched, the area per lipid is larger (compared to lower temperatures) and the lipids have greater lateral mobility.

This phase is called the liquid disordered phase, fluid phase or, as will be used in this writing, L_α. As the temperature of the lipid bilayer is lowered, starting from high temperatures, a phase transition $L_{\beta'} \rightarrow L_\alpha$ is observed. The temperature at which this happens is called the transition temperature T_m. This transition is a melting and corresponds very well to other melting processes when pictured. At low temperatures most materials are in their solid phase with movement of the molecules restricted and the rigidity of the material is high. As the material melts the molecules becomes more mobile and the rigidity of the material falls dramatically.

A phase diagram for DOPC:DPPC[1] can be seen. On the horizontal axis the molar fraction of DPPC (X_{DPPC} is displayed an don the vertical axis the temperature T. The diagram maps pairs of X_{DPPC} and T to a phase. For example will a bilayer consisting of a 1:1 mixture ($X_{DPPC} = 0.5$) of DOPC:DPPC at a temperature $T = 40°C$ be in the L_α phase. As this bilayer is cooled of it will at $T = T_m \approx 34°C$ begin to divide into two phase. The $L_{\beta'}$ phase begins to solidify and coexist with the L_α phase. This region of the phase diagram is called the coexistence region for this reason. The solid $L_{\beta'}$ will group together in certain areas and this is what is called a gel domain or $L_{\beta'}$ domain. In vitro vs model membrane The molar fraction of lipids in each phase, and the composition of those phases, can be determined via the level rule. Tielines for determining this have been drawn on the DOPC:DPPC phase diagram for $T = 20°C$ and $X_{DPPC} = 0.5$. The amount of molar fraction of lipids in the solid $L_{\beta'}$ phase $X_{L_{\beta'}}$ and the molar fraction of lipids in the liquid L_α phase X_{L_α} are given by:

$$X_{L_\alpha} = \frac{W_s - X_{DPPC}}{W_s - W_l} \tag{1}$$

$$X_{L_{\beta'}} = \frac{X_{DPPC} - W_l}{W_s - W_l} \tag{2}$$

These equations are simply the the length of the two piecse of the blue dash line, separated by the green dashed line, divided by the length of the blue dashed line. That is where the name lever rule comes from.

Other phases than L_α and $L_{\beta'}$ exist, but they are not of interest in this thesis. Neither will they interfere with the phases that are of interest because they take place at much lower temperatures or under other experimental conditions. As an example the ripple phase $P_{\beta'}$ lies, temperature wise, between the L_α and $L_{\beta'}$ phase but it is almost completely suppressed in supported bilayers due to coupling between the substrate and the membrane[3]. It can however be observed in the 2nd bilayer (e.g. if the extra bilayers were not rinsed away before cooling the sample down).

The phase transition $L_\alpha \rightarrow L_{\beta'}$ is happening individually for each leaflet of

[1]The diagram is for giant multilamilar vesicles of DOPC:DPPC, not for supported bilayers as this thesis is concerned with. More on this later.

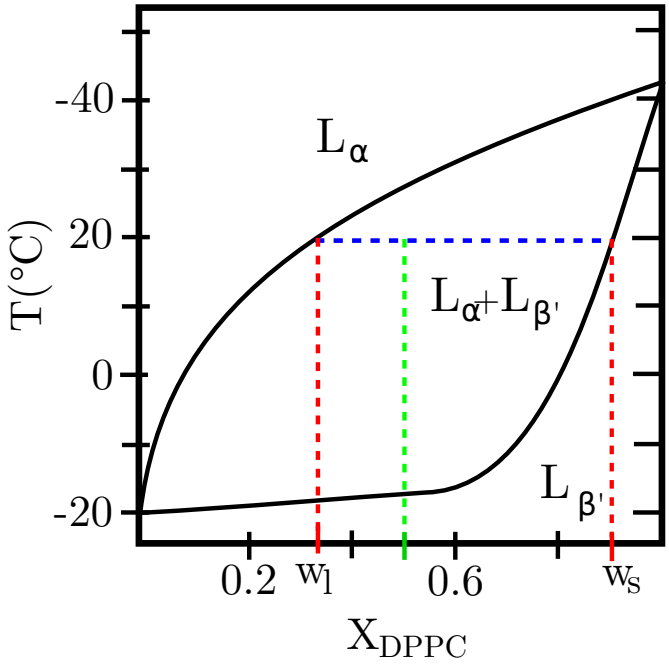

Figur 3: Phase diagram for a giant multilamilar vesicles made of a DOPC:DPPC mixture. Tielines displayed for $T = 20°C$ and $X_{DPPC} = 0.5$ (1:1 mixture). Redrawn from [4] for illustration purposes.

the bilayer. If the bilayer is not coupled to its surroundings (e.g. a solid support) the transition temperature will be the same for the two leaflets and they will undergo the phase transition simultaneously. If bilayer does not exist free of its surroundings the leaflets might transition at different temperatures. This has been observed to be the case for bilayers of mixtures of DPPC and 1-stearoyl-2-oleoyl-sn-phosphatidylcholine (SOPC)[5]. This is due to interactions between the headgroups of the proximal leaflet and the substrate. The effect is however not observed when the bilayer is immersed in buffer solutions with ions present[6]. The headgroups of the lipids are often zwitterionic and the presence of other ions might screen the proximal leaflet from the solid support.

1.2 Nucleation of domains and defect centers

In classical nucleation theory (CNT) nucleation in two-dimensional systems is a balance between the energy gained by forming a nucleation site and the energy cost of creating a line interface:

$$\Delta G = \pi r^2 \Delta G_A + 2\pi r\gamma \tag{3}$$

where δG is the free energy needed to create a new circular nucleation site, r is the radius of this nucleation site and γ the line tension between the liquid phase and the solid phase. ΔG_A is a negative quantity measuring the energy

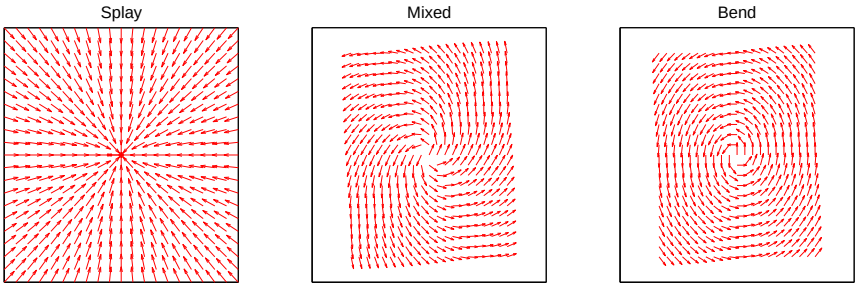

Figur 4: The three orientational fields that can be generated by a +1 point defect.

released by creating a nucleation site. A critical radius can be calculated which is the radius a nucleation point needs to reach to become stable. The line tension between the two phases comes from a hydrophobic mismatch between the lipids in the liquid phase and the lipids in the solid phase. The nucleation phenomenon of meta stable nucleation spawning and disappearing for binary lipid mixtures plays out on length scales which are much too small to be resolved optically with a microscope. It can however be reproduced by molecular dynamics (MD) simulations[7]. Here small, short-lived, meta-stable nucleation points are seen to exist as the phase transition temperature is reached and lowering the temperature a little more cause stable nucleation sites to form and grow.

Little else is known about nucleation in solid supported lipid bilayers as they are forced through the phase transition by cooling the bilayer. Very recently attempts to construct a nucleation theory involving the rate of cooling have been made by one of my supervisors and one of of his students. They quantify the nucleation density as function of the cooling rate. [8]. This work will not be discussed here since this thesis is not concerned with the nucleations per se, but merely accept it as an input for the growth of the domains.

From experiments[12, 20] it is known that a point defect is present in the center of the domains. This point defect is actually two close lying point defects, but at long distances away from the center the orientational field look as if it were a single point defect. This point defect can generate three distinct orientations fields: pure bend, pure splay and a mix of the two. These are shown on figure 4. These are the type of textures that will be found in the gel domains in the experimental section.

2 Preparation and characterization

2.1 Preparation of supported lipid bilayer membranes

Several methods exist for preparing supported lipid bilayers. Three common methods are briefly described below.

2.1.1 Transfer of monolayers from air-water interface (Langmuir-Blodgett / Langmuir-Schaefer method)

Using this method a lipid monolayer film of the desired composition is first prepared on an air-water interface in a Langmuir trough. Then the desired substrate, for supporting the membrane, is brought into contact with the monolayer such that it is deposited on the surface. If the substrate is dipped horizontally into the monolayer film then it is called a Langmuir-Blodgett film whereas if it is dipped vertically it is called a Langmuir-Shaefer film. Both methods deposit one monolayer per iteration, so to create a bilayer the sample would have to be dipped twice. The result is very uniform coating of the substrate.

An advantage of this method is that the composition and packing of each leaflet of the bilayer can be controlled independently of the other. This can however also be an disadvantage since the two leaflets are decoupled during their creation. This could lead to different packing compared to bilayers formed using other methods.

2.1.2 Vesicle fusion

This method utilizes the fusion of small unilamilar vesicle (SUV) to the substrate. SUVs are first formed in a solution and the substrate then exposed to the solution. Attractive forces between substrate and lipids cause the SUVs to fuse to the substrate. The result of this process is non-uniform coating of the substrate and subsequent rinsing of the sample to flush away excess SUVs is most likely needed. An advantage of this method is the ability to incorporate proteins into the membrane. SUVs can be prepared such that they contain membrane proteins which will remain embedded in the membrane after it fuses to the substrate [9].

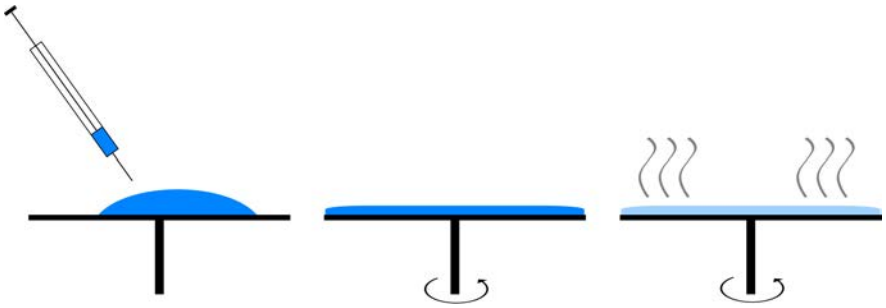

Figur 5: The three steps of spin-coating, left to right: 1) Application of the lipid solution, 2) Excess solution removed by spinning, 3) evaporation of remaining solvent.

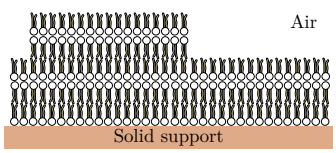

(a) The try lipid film in air.

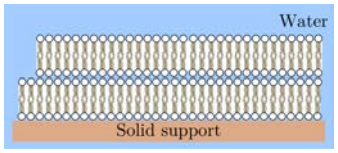

(b) The fully hydrated lipid bilayer.

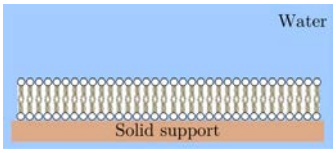

(c) Hydrated lipid bilayer after rinsing.

Figur 6: The three steps needed to obtain a single supported, hydrated lipid bilayer.

2.1.3 Spin coating

In this thesis the method used for preparing supported lipid bilayers is spin-coating. Spin-coating is a general technique for depositing thin films on flat surfaces. It is widely used in microfabrication for coating silicon wafers for photolitography, but can also be used to deposit thin films of lipids on flat substrates [10]. In this technique the substrate is attached to a rotating device as depicted in figure 5. Using a pipette, or similar, a small amount of lipid solution is placed at the center of the substrate. The substrate is then spun at high speed (3000 rpm). The centrifugal force spreads the lipid solution uniformly over the substrate and causes excess solution to leave the substrate. This creates a thin film of solution which can evaporate while the spinning continues. The balance between viscous forces in the solution, adhesive forces between substrate and solution, and the centrifugal force dictates the thickness of the film. This technique have been show to create thin lipid films of high quality[11].

There are two main requirements for the solvent for this technique to work: the desired lipids need to be soluble in it and it needs to wet substrate properly. A mixture of hexane and methanol (97:3 by volume) works well for most lipids and glass or mica substrates[12]. After spin-coating the substrate is placed in an exicator ($P \approx 0.1atm$) to ensure that all organic solvent is evaporated and the film completely dry.

The dried film is depicted in figure 6a. Even though depicted as such no bilayers, like those found in aqueous environments, are present at this point in time. The bilayer structure is a result of the hydrophilic headgroups and hydrophobe tails. When no water is present there is no energetic advantage in forming such structures. So the lipids are most likely in no particular ordered state. The dry film is then hydrated by placing the spin-coated substrate in an aqueous solution. As soon as the lipids are experiencing the presence of water they minimize their TODO free energy by forming bilayers (figure 6b). TODO slighly decoupled show picture if one can be found. When fully hydrated the solid support will be covered in multiple bilayers (2-3) and to obtain a single bilayer attached to the solid support those extra bilayers needs to be rinsed away. This is simply done by flushing the sample with the same aqueous solution using a pipette. The rinsed away bilayers drift around in the aqueous solution, possibly as micelles since they are no longer forced to be planar by the substrate, and will attach to the membrane again if not removed. The only way to remove them is to dilute the aqueous solution with more fresh solution to a point where no significant amount of drifting membrane is left.

2.2 Characterization

2.2.1 Fluorescence microscopy and confocal laser scanning microscopy

This is a short introduction of the fluorescence microscopy and laser scanning microscopy technique which is used in the work to visualize the lipid membrane. It is basically a summary of what can be found in a book on the subject, for example [13].

In fluorescence microscopy the image is not created by reflection and absorption of the source light by the sample, but by light emitted from fluorescent molecules embedded in the sample. The fluorescent molecules embedded in the membrane will from now on be called (fluorescent) probes or dyes. A fluorescent absorbs light at one wavelength and emits light at another longer wavelength. The absorption and emission spectrum of a fictitious probe is shown in figure 7b. For a probe to be useful for fluorescence microscopy the change in wavelength of peak absorption intensity and peak emission intensity needs to be large enough to allow the two wavelengths to be separated using longpass or bandpass filters.

The setup used for this work was an epifluorescence microscope setup where the same light path is used for illumination of the sample and image formation on the detector. Such a setup is shown schematically in figure 8b. A light source is used to excite the probes embedded in the sample. The light source can either be tuned to the peak excitation wavelength or it can emit a broad spectrum

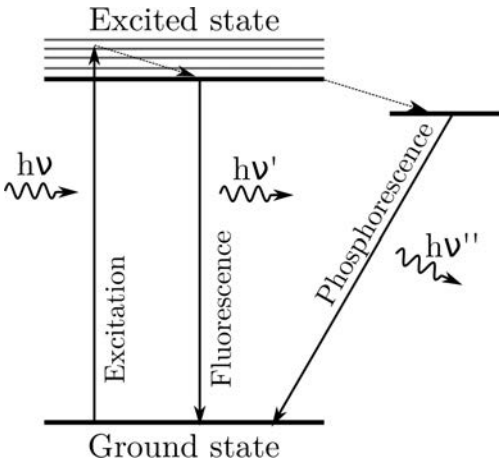

(a) Jablonski diagram showing excitation of a dye molecule by an incomming photon and subsequent emission of a new photon by either fluorescence or phosphorescence.

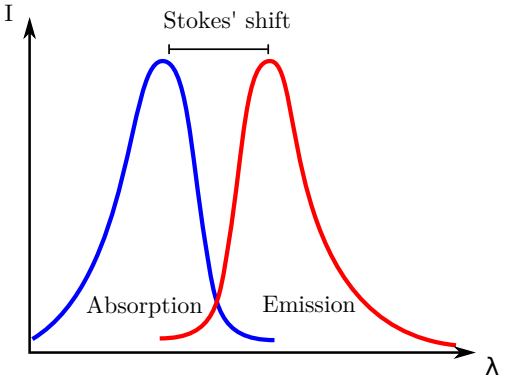

(b) The difference in wavelength between peak excitation and peak emussion wavelength is called the Stokes' shift.

of wavelengths, e.g. white light, which can be narrowed down to the desired excitation wavelength by the excitation filter. The light is then reflected towards the sample by a dichoric mirror or beam splitter, and is finally focused on the sample by the objective. The disadvantage of a beamsplitter is that intensity of the source light is lost since only some of it (e.g. 50%) is reflected towards the sample. A dichoric mirror reflects specific wavelengths and transmits others. Dichoric mirros can therefor be made to reflect the excitation wavelength and transmit the emission wavelength which reduces the loss of intensity significantly. The light then then excites the probes and the probes emit light at a shifted, longer wavelength. This light is emitted in all directions and some of it travels back into the objective. Some of the excitation light is also reflected or scattered back into the objective. The light then passes the dichoric mirror again where any remaining light of the excitation wavelength is reflected back towards the source and the light with the emission wavelength is transmitted. If the dichoric mirror is not enough to separate the two wavelengths from each other the emission filter can be chosen to correct for any shortcomings of the dichoric mirror. The light is then detected by the detector and an image is formed.

The detector can be of different types: a camera, an eye or a photomultiplier (PMT). In this project both wide field imaging and confocal imaging of the sample was used. For widefield imaging the detector is a camera and the image is formed just as with any digital camera. The image of the sample have to be focused on the camera's CCD or CMOS array by the objective. The light source for wide field imaging is typically a broad spectrum lamp or LED since illumination of the whole samples is required simultaneously. Lasers could be used, but their beam profile and spacial extend make them more suitable sources for confocal imaging.

Confocal imaging is an imaging technique that optical resolution and contrast by using point illumination and spatial pinhole to eliminate out-of-focus light in samples that are thicker than the focal plane. This provides much better spacial resolution than normal wide field imaging which illuminate the whole sample surface and collects light emitted from all depths of the sample. The light source is typically a laser since their collimated light is already much more spacially confined than a normal point source and it is easier to reach high intensities. The confocal technique used in this project is confocal laser scanning microscopy (LSM). In this technique the laser is scanned across the sample illuminating one point at a time. The scanning is done by two oscillating mirrors which by changing the angle of incidence of the laser beam alters its position on the sample. One mirror scans it horizontally and the other vertically. Since only one point is illuminated at a normal wide field detector such as a camera cannot be used to directly form an image of the illuminated sample. The spacial information about which point emitted the detected is not available by just looking at the emitted light collected by the objective. So instead all light collected by the objective is detected by a single PMT and its spacial position in the final image is given by the position reported by the controller of the scanning motion at time of detection. Pairs of intensity and positions are collected during the scanning and later, typically by software, the pairs of intensity and position is made into an image. Figure 8a shows the part of the sample which is scanned and mapped to an image. A square region of the sample measuring $b2L \cdot 2B$ is chosen and divided into N rows and M columns. The laser is then moved in steps of $\frac{2L}{M}$ horizontally and $\frac{2B}{N}$ vertically. Each point is illuminated for a predetermined amount of time, the exposure time, and the intensity recorded by the PMT. The intensity at a given point is $I_{i,j}$ for $i \in [0, N]$ and $j \in [0, M]$. This intensity can afterwards be mapped directly to an N by M pixel digital image with the gray scale value of pixel $P_{i,j} = I_{i,j}$. The resolution of the image is given horizontally by $\frac{2L}{M}$ and vertically by $\frac{2L}{M}$. Keeping L and B constant and increasing N and M will make each pixel map to a smaller physical area of the sample, and vice versa. The limiting factor resolutionwise is how much the laser beam can be focused on the sample. It gives no further resolution to sample more than once within each illuminated area. This technique is used for imaging the Laurdan probe in the samples.

The axial resolution of the confocal technique can be further improved by using two-photon excitation instead of one-photon-excitation. Instead of the fluorescent probe being excited by absorption of a single photon with the required energy it can be excited by simultaneous absorption of two photons with approximately half the required energy. The probability of a two photon excitation is proportional to the intensity squared $P_{\text{two-foton}} \propto I^2$ compared to $P_{\text{one-photon}} \propto I$. for one-photon excitation. This means that the ratio of excitation events, and hence fluorescent emission events, taking place at the narrow beam waist to the excitation events taking place axially farther away from the beam waist goes up. Observe for example the beam waist depicted in figure 7. With one photon exci-

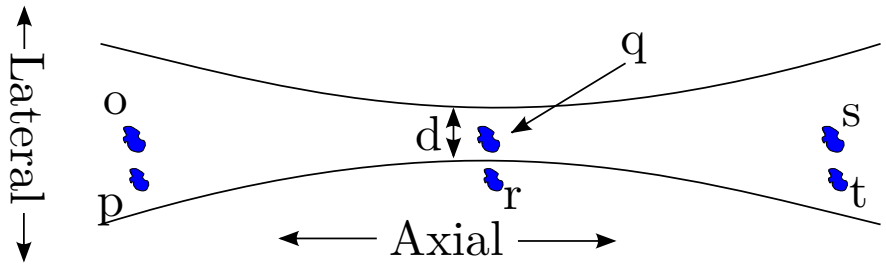

Figur 7: The waist of a focused beam of light. Objects o and p, as well as s and t will appears as one object laterally whereas q and r will appear as two objects. Axially o,q and s will all contribute to the same object int he image, and p and t will contribute to another object. The Abbe difraction limit $d = \frac{\lambda}{2(n \sin\theta)}$ is also marked.

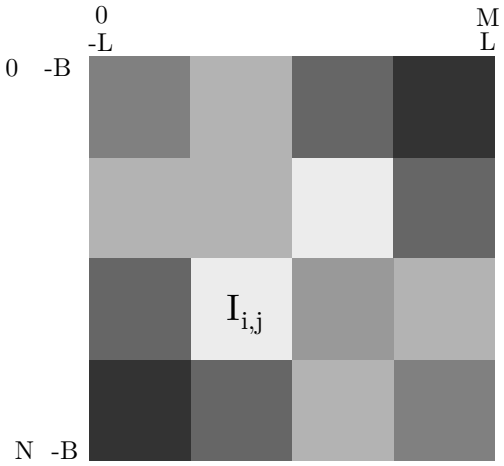

(a) The virtual grid of the LSM technique. Each grid section corresponds to a location on the sample and a pixel in the digital image created.

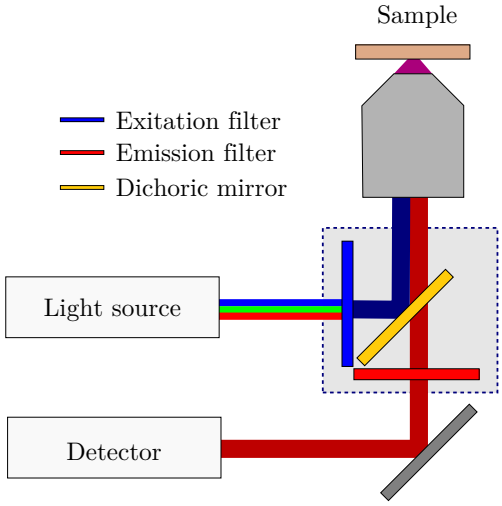

(b) Schematic of an epifluorescence microscope. Shown are the light paths from light source to sample and sample to detector.

tation the probe o and probe s would contribute more to the total intensity of that lateral position, then they would with two-photon excitation. So axial resolution is improved further by concentrating the excitation events at the beam waist axially. Another advantage of two-photon excitation is that the photons carry less energy per photon and therefor they tend to cause less damage to the sample being imaged.

2.2.2 The Laurdan and DiD fluorescent probes

First and foremost a probe were needed to visualize the orientational texture of the $L_{\beta'}$ domains in the lipid membrane. Such a probe should partition into the $L_{\beta'}$ phase, be sensitive to the lipids tilt and if it also partitions into the L_α phase

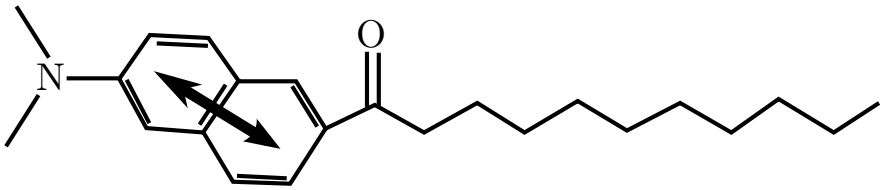

Figur 8: The Laurdan probe consist of a hydrophobic fatty acid tail linked to a hydrophilic naphthalene molecule. The naphthalene molecule has a dipole moment indicated by the black double-headed arrow.

the signal from the two phases should be distinguishable.

6-Dodecanoyl-2-Dimethylaminonaphthalene (Laurdan) does all those things. It partitions into both the $L_{\beta'}$ and the L_α phase, but its emission wave length is shifted from one phase to the other which allows the signals to be distinguished. Laurdan is excited at $\lambda = 363nm$ for one photon excitation[14] or $\lambda \approx 750nm$ for two-photon excitation. In this work two-photon excitation at $\lambda = 780nm$ was used. The emission wave lengths are $\lambda_{L_\alpha} = 475nm$ and $\lambda_{L_{\beta'}} = 440nm$[12, 15]. Since two PMTs were available on the microscope it was possible to record both signals and the setup easily allowed splitting the signal using a dichoric mirror which transmits $\lambda > 465nm$ and reflects $\lambda < 465$. However only the channel containing the data for the $L_{\beta'}$ phase was optimized and recorded.

The Laurdan probe, shown on figure 8, consist of a hydrophobic fatty acid chain linked to a hydrophilic naphthalene molecule. This cause the probe to align itself with the lipids making up the membrane. The naphthalene molecule (a pair of benzene rings) experience partial charge separation and therefor has a dipole moment. When illuminated this dipole is excited and it is responsible for Laurdans fluorescence. The dipole is more likely to be excited by photons whose polarization aligns with the dipole, so illuminating the sample with linearly polarized light (lipid membrane with Laurdan embedded) will cause those Laurdan molecules whose dipole align with the polarized light to emit more photons and stand out from the rest whose dipole do not align. This is what makes Laurdan good for visualizing the tilt of the lipids surrounding it[16, 17]. More on this in section 2.2.3.

The other probe needed is for quick inspection of the membrane during sample preparation and for long-term visualization which would bleach the Laurdan probe away. This probe should be able to exist in the membrane along with Laurdan without overlapping it's excitation spectrum or emission spectrum. The former would cause both probes to be exited and Laurdan to be bleached anyway, the latter would make it impossible to filter out the Laurdan signal. It should also partition into only one of the phases, otherwise it would not be possible to distinguish them.

1,1'-Dioctadecyl-3,3,3',3'-Tetramethylindodicarbocyanine (DiD) have these properties. It partitions into the L_α phase and makes the $L_{\beta'}$ domains appear dark on a bright background[18]. Its excitation peak is for $\lambda = 644nm$, but at $\lambda \sim 550nm$ it still absorb enough to be excited[19]. The excitation with yellowish-green light stays well away from Laurdan one- or two-photon peak excitation wave lengths. Its peak of emission is at $lambda = 664nm$ which is also well away from the Laurdan emission wave lengths.

2.2.3 Texture measurements and visualization

As mentioned in section 2.2.2 the Laurdan probe contain a dipole which is the source to its fluorescence. The orientation of the dipole depends on the orientation of the Laurdan probe as a whole, and since Laurdan aligns its fatty acid tail with the surrounding lipids the dipole orientation depends on tilt of the surrounding lipids. The chance of exciting the dipole is larger the better the polarization of the light aligns with dipole. Hence by illuminating the sample with linearly polarized light a stronger response is seen from the Laurdan molecules whose dipole align with the polarization of the light. When rotating the polarization of the illuminating light different Laurdan probes will give of the strongest signal. If the polarization is rotated a full 2π, in suitable steps, all orientations of the dipole will have been probed.

A texture measurement therefor consist of taking a series of images while illuminating the sample with light of changing linear polarization. Figure 9a and 9b show two individual images, from an image series, with orthogonal polarizations. The most bright leaf have its Larudan dipoles aligned with the polarization used for these image. As seen, different leafs of the domain light up for different polarizations. The sum of all 18 images in the given series is seen in figure 9c and here the domain is more easily recognizable as a rosette with five leafs.

The raw images them selves give some indication that the orientation of the lipids vary thoughout the domain, but noting quantitative can be extracted from the images using the naked eye except that the leafs seem to change intensity periodically. This periodic phenomenon can be quantified by computing the discrete Fourier transform the image series. This method is described in [20] and below it is summarized:

For each pixel in each image in the series an intensity I_k is defined as

$$I_k^{mn} = I^{nm}(\phi_k) = I^{mn}(\phi_{offset} + R \cdot k \cdot \Delta\phi) \tag{4}$$

where m and n refer to the row and column in which the pixel is located in the image and k refer to the image number in the sequence of images or the current angle of polarization. $R = \pm 1$ indicates the direction of rotation. $R = 1$ means

counter-clockwise rotatio. This means there for each pixel will be a set of $N = \frac{2\pi}{\Delta\phi}$ intensities I_k^{mn}. For each of these sets the discrete Fourier transform is computed as:

$$\tilde{I}_\gamma^{mn} = \sum_{k=1}^{N} I_k \cdot e^{-i2\pi\frac{1}{N}(\gamma-1)(k-1)} \tag{5}$$

This gives N unique Fourier modes. For a noise free $I(\theta) = cos(\theta)^4$ signal I_3^{mn} corresponds to the only sine term in the Fourier series with non-zero amplitude. When noise is present in the signal the other modes will become non-zero as well. The amplitudes and phase of the sine terms are:

$$\text{Amplitude: } \frac{|I_\gamma^{nm}|}{N} = \sqrt{Re(I_\gamma^{nm})^2 + Im(I_\gamma^{nm})^2}$$
$$\text{Phase: } atan2(Im(I_\gamma^{nm}), Re(I_\gamma^{nm}))$$

The magnitude $L^{mn} = |I_\gamma^{nm}|$ is denoted the director length. The director angle is the dominant angle of the probe director within a single pixel. Taking direction of rotation and polarization scanning offset into account this angle is given by:

$$\varphi_c^{mn} = -\frac{1}{2} \cdot R \cdot arg[I_\gamma^{nm}] + \phi_o ffset \tag{6}$$

The texture of the domain is the image of φ_c^{mn}. This angle only makes sense for the gel domains where the lipids are tilted in an orderly fashion. In the liquid disordered phase this angle will shift randomly from pixel to pixel indicating that there is no orientational order in the L_α phase. The director angles will be distributed over the interval $[\frac{-\pi}{2} + \phi_{offset}, \frac{\pi}{2} + \phi_{offset}]$. The reason for this is that one probe director can not be distinguished from another probe director which is rotated π. Those two dipoles will have the same affinity for a given angle of polarization. It is also important to note that the director angle is not the zenith or inclination angle of the lipids, but closer to their azimuth angle. This technique cannot determine the true molecular tilt, only some indication of it's projection in the plane of the membrane.

Figure 9d shows the analyzed texture for the domain. The black bars indicate the angle of the probe director and the color is the mapping of the director angles to HSV color space. $[0, \pi]$ is mapped to the HSV color space and hence each color appears twice, for ϕ_c^{mn} and $\phi_c^{mn} + \pi$. The length of the black bars is the director length L^{mn}. Unless otherwise explicitly stated "texture"in this work will refer to the image of the director angles only.

2.3 Experimental procedures

All experimental activity presented in this thesis is centered around the same supported lipid bilayer sample. The following sections will describe how arrive

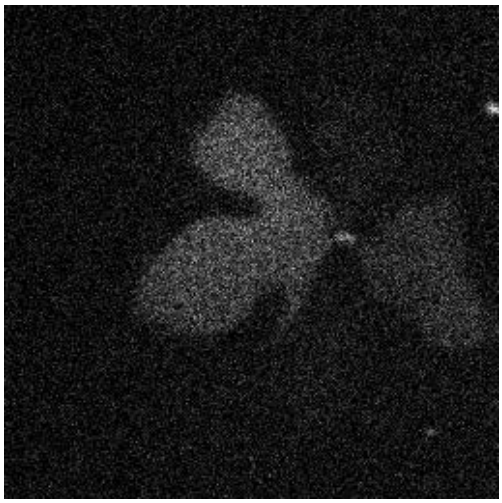

(a) One individual images making up the sum in figure 9c.

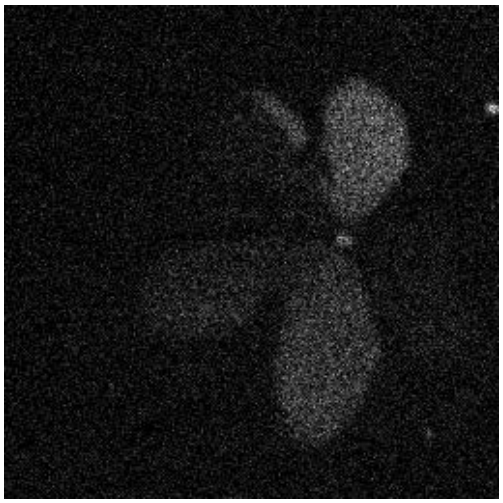

(b) Another individual image with polarization orthogonal to that in 9a

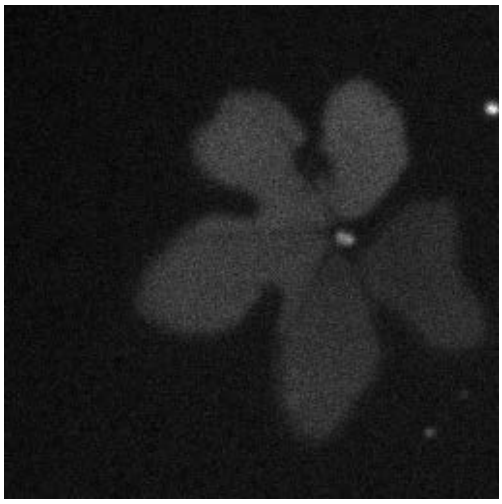

(c) The sum of all 18 or 36 images from the rotation scan.

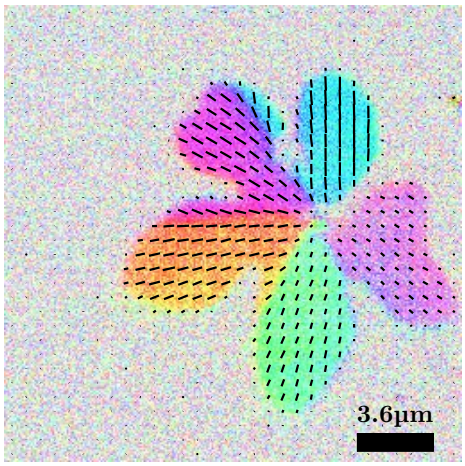

(d) The image of the director angles and lengths.

Figur 9: 9c: The gel domain is rosette formed. 9a: One of leafs on the rosette is significantly more visible than the others. The lipids in this leaflet are tilted such that the Laurdan dipole is aligned with the polarization of the light in that image.

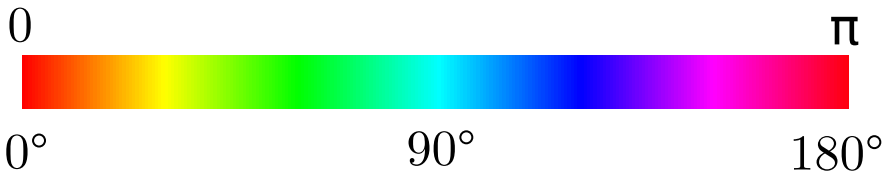

Figur 10: The director angles are mapped to the HSV color space.

at the fully prepared sample shown in figure 11. Unless stated otherwise the experimental choices (lipid mixtures, cooling rate etc.) are made to mirror those found in [12]. It will describe both the equipment and materials used as well as the procedures.

2.3.1 Dry film from spin-coating

Pieces of Muscovite mica sheets are used as supporting substrate for the lipid bilayers. The sheets are purchased from Plano GmbH, Germany, and have the same size as a regular microscope slide. From those sheets square $1cm^2$ pieces were cut using a pair of standard office scissors. Pieces of glass a little larger than the mica pieces were cut from standard microscope slides, thickness $1mm$. Attaching the mica to the glass was done using biocompatible silicone glue (MED-6215, Nusil Technology, Santa Barbara, CA TODO). The silicone glue have the advantage of remaining flexible after curing which cause less stress to build up in the glass and mica pieces and being biocompatible it is not likely to give of any molecules which could interfere with biological membrane. The mica is attached to the glass to provide easier handling of the sample with tweezers and to ensure that any lipid film present on the backside of the sample will be sufficiently long away from the surface of interest the two do not share the same focus plane.

Immediately prior to the spin-coating the mica sheet, now glued to the glass, was cleaved using a scalpel. Gently inserting the edge of the scalpel into the edge of the mica near a corner will cause a layer of the mica to come loose, exposing a clean, dust and scratch free surface.

The spin-coating is done as described in section 2.1.3. The lipid solutions used for the spin-coating were:

- $10mM$ DOPC:DPPC (1:1)
- $10mM$ POPC:DSPC (2:1)

Both sample solutions had $\sim 0.5\%_{mol}$ Laurdan and $\sim 0.5\%_{mol}$ DiD added to allow visualization via fluorescent microscopy. The sample solutions were prepared as needed from $10mM$ DOPC, DPPC and DSPC stock solutions. These solutions were made by dissolving dried lipid powder, purchased from Avanti Polar Lipids, Inc., USA, in a 97:3 (by volume) mixture of hexane and methanol. These are stable for a long time when kept in a freezer at $\sim -20°C$ and can be used for at least a year to create mix new sample solutions with varying composition. The sample solutions were typically made in $1mL$ batches and were just kept int he freezer as well when not used for spin-coating. Prior to spin-coating the samples solutions were removed form the freezer, allowed to heat to room temperature and stirred

thoroughly to ensure that all lipids were dissolved. When cooled below room temperature the lipids start to precipitate. $\sim 30\mu L$ lipid solution was used for spin-coating. The samples spun at $\sim 3000rpm$ for 40 seconds. After spin-coating the samples were placed in a plastic Petri dish, wrapped in tinfoil to keep out light, and placed in an exicator for at least 30 minutes, but they can remain there, and still be usable, for at least a week.

2.3.2 Hydration and rinsing

After exication the sample was moved to a Petri dish suitable for use on the microscope and the Petri dish filled with $\sim 5mL$ HEPES buffer ($pH = 7$,ionic strength $0.15M$). The initial temperature of the buffer was usually $\sim 20°C$, but could range rom $5°C$ to $50°C$. The whole assembly was then heated to $60°C$, an arbitrary temperature above the melting point of DOPC, DPPC and DSPC, for 60 minutes to ensure full hydration before being rinsed.

The rinsing was done with $\sim 80°C$ HEPES buffer to ensure the temperature did not drop below the melting point. During rinsing the membrane was inspected with a normal wide field camera, attached to the microscope, imaging the DiD probe, to ensure it was rinsed enough to leave a single bilayer on the substrate. Between each inspection of the membrane during rinsing the $\sim 5mL$ volume of the Petri dish was exchanged 2-5 times to remove drifting membrane. The whole rinsing procedure uses $\sim 100mL$ of buffer. After rinsing, prior to cooling, the Petri dish ensemble was allowed to equilibrate to $60°C$ again.

Due to the fact that the mica solid support is birefringent the samples have to be turned upside down so the membrane faces towards the bottom of the Petri dish and the objective. The linear polarization of the excitation light will be changed by passing through the mica. This is done after the rinsing of the sample and before further heating/cooling.

2.3.3 Heating and cooling of the sample

The heating of the Petri dish ensemble was done using a Peltier element fitted to a flat disk, designed to heat/cool normal microscope slides. The disk with cords to power the Peltier element and tubes to supply water as heat exchanger to the Peltier element fit the microscope stage and still allowed movement of the objectives etc. To ensure proper thermal contact between the flat disk and the Petri dish a custom aluminum block was fabricated to closely fit the Petri dish and cover a larger surface area of the Peltier element disk. Between the disk and aluminum block thermal paste were applied to ensure proper thermal contact. Since the controller of the Peltier element did not feature an external

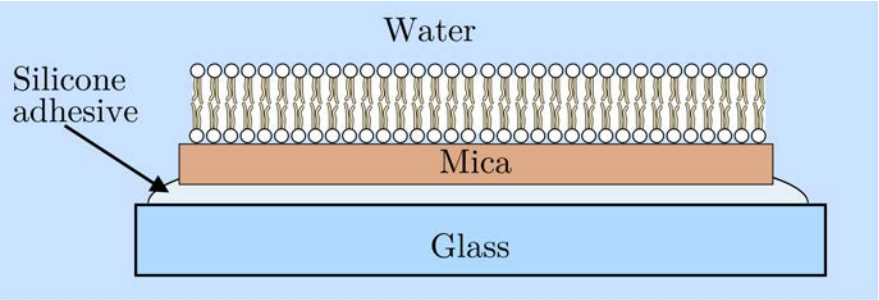

Figur 11: The different layers of a fully prepared sample immersed in aqueous buffer solution. The schematic drawing is not to scale.

thermal sensor to control the output of the Peltier element, the temperature in the water in the Petri dish had to be carefully calibrated against the temperature set points of the Peltier element. The cooling rate of the peltier element also needed calibration against the actual cooling rate of the water in the Petri dish. By carefully choosing the cooling ramp profile on the Peltier controller a linear cooling profile with a chosen slope (rate) could be generated in the water.

After equilibrating back to $60°C$ after rinsing the ensemble was cooled to a temperature below the melting point lipids forming the $L_{\beta'}$ phase (DPPC and DSCP) at a rate of $1.0\frac{°C}{min}$ to grow the gel domains. The temperature to which the samples were cooled are dictated by a few things: it has to be below the L_α to $L_{\beta'}$ transition temperature, and it has to match the temperature of the surroundings, especially the temperature of the objectives of the microscope. Since water immersed objectives were used for the LSM they act as a heat sink in *very* good thermal contact with the sample. So trying to keep the sample at $20°C$ using the Peltier-element while being in contact with a $\sim 28°C$ objective was futile. The sample would end up having a temperature in between, and probably closer to the temperature of the objective than that of the bulk water which is in equilibrium with the Peltier element. The temperature of the objectives were monitored with an ad-hoc attached thermocouple. The temperature of the objectives was found to vary several degrees depending on which detectors, mounted on the microscope, were running and steps were taken to cool the objectives to to $T = 20°C$. This was done by wrapping the mounted objectives in thin plastic tubing and circulating cold water through the tubes. If the temperature of the sample and the objective is not matched you either melt part of or further grow the gel domains after they come into contact with the objective which could potentially alter the shape of the domains.

2.3.4 Texture measurement

As described in 2.2.3 the experimental steps of a texture measurement is to take a series of images of the membrane while it is being illuminated by light with

changing linear polarization. Imaging of the Laurdan probe is, as described in section 2.2.1, is done with two-photon, confocal LSM. The light source used is an TODO laser tuned to $\lambda = 780nm$. To obtain linear polarized light a linear polarizer is inserted into the light path leading to the microscope. The polarizer is attached to a motor which can rotate it in programmable steps. The controller of this motor has a triggering mechanism which is connected to the triggering output of the controller for the scanning mirrors. It emits a pulse each time it has scanned a complete image. Upon receiving this trigger pulse the motor controller rotates the polarizer one step. The motor controller can be programmed to take steps $\Delta\Phi$ of desired length and in which direction it shall rotate.

Before the system can be used to record images, which can be used for texture analysis, some calibration is needed. The angle of the linear, rotatory polarizer (e.g. the angle of the linear polarized light) needs to be calibrated against the orientation of the sample on the microscope. The orientation of the sample on the microscope in turn needs to be calibrated against the orientation of the images recorded. This is needed to determine the direction of rotation and the offset angle ϕ_{offset}, both needed for the texture analysis procedure. Calibrating the polarization angles is done simply by replacing the sample on the microscope with another linear polarizer which is then rotated until maximum or minimum of transmission is detertments cted. This gives a mapping between the angle of the motorized polarizer and the microscope stage. Calibrating the orientation of the sample on the stage against the orientation of the sample in the recorded images is done by replacing the sample with an easy to identify asymmetric object. Then orientation of the object on the stage is simply compared to the objects orientation in the image.

Once all the calibration is done a sample is prepared as described earlier and placed the microscope. After it has been rinsed and cooled of to $T \sim 20°C$ the membrane is first inspected with a camera and the DiD probe to get an overview of the sample. This can be done with air objectives and 20x magnification. Once the sample is confirmed to have grown domains of observable size the objective is switched to a 60x water-immersed objective. A droplet of purified water is placed on the objective and given a minute to equilibrate its temperature against the objective's. Then sample is brought into focus and once an interesting area of the sample have been found with the camera the microscope is switched to laser scanning mode. The focus of the LSM is slightly different from that of the camera and lamp. A few low resolution, low exposure scans are made of the sample to bring it into focus again. When LSM focus is established the motorized polarizer is verified to be in it's calibrated starting position, the intensity of the laser is increased and the resolution of the scanning increased before the automatic image acquisition process is started.

2.3.5 Long-term, time-resolved imaging of membranes

Some long-term/long-duration, time-resolved experiments were performed by leaving the samples on the microscope for an extended period of time.

Acquisition of DiD wide field images could be completely automated using Micro-Manager[21] to control the microscope and camera. Using Micro-Manager images could automatically be acquired at regular time intervals and at multiple locations on the sample utilizing the motorized XY-stage mounted on the microscope. Perfect Focus, an Olympus automated focus system, was used to keep the sample at a constant distance above the objective to avoid the sample drifting out of focus. The objective used was either a 20x or 40x for use in air. At the time of these experiments the setup for doing texture measurements were in high demand and it was not possible to use this microscope for several days at a time for this purpose. The samples for these experiments therefor had to be prepared on one microscope and then moved to another for the long-term imaging. The temperature control apparatus described in section 2.3.3 did not fit the stage of this secondary microscope, so the two different temperature control systems had to be calibrated against each other to ensure the temperature of the sample stayed constant when moved from one microscope to the other.

Automated acquisition of the images series used for texture analysis was not possible within the time frame of the project. So that had to be done manually. The challenges for automating this task is application of water to the water-immersed 60x objective and stable operation of the motorized rotatory linear polarizer. The water covering the objective needs to be reapplied every few hours and the motorized polarizer tend to drift when reversing to its zeroed position.

3 Experimental results

In this section the size, shape and texture of the gel domains will be presented at different stages of their existence; starting with the domains as they grow and ending with the domains after the membrane have been stored for more than two months.

3.1 Domain growth

The growth of the gel domains were investigated qualitatively using DiD probe and wide field imaging. Figure 12 shows the gel domain as they grow in a DOPC:DPPC bilayer (1:1 mixture). The domains become visible through a 20x

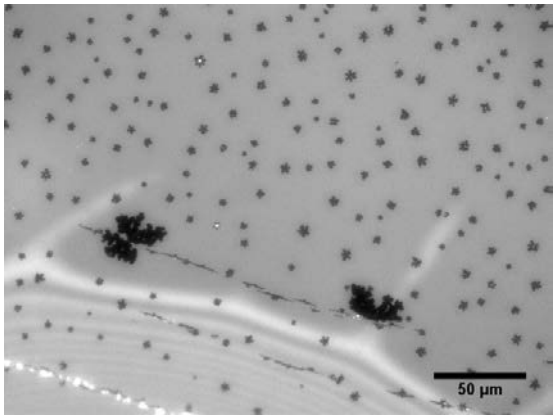

(a) The membrane shortly after reaching the transition temperature $T_m \approx 34°C$.

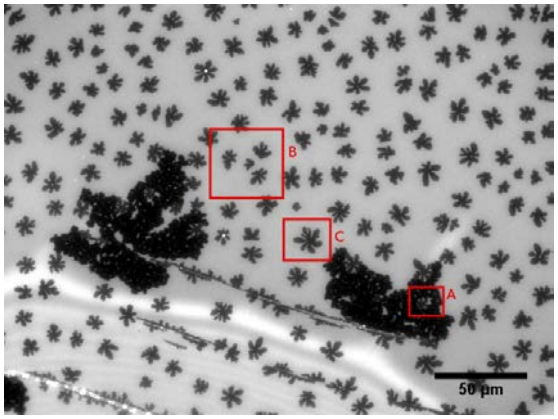

(b) The membrane shortly after the temperature had stabilized at $T = 20°C$.

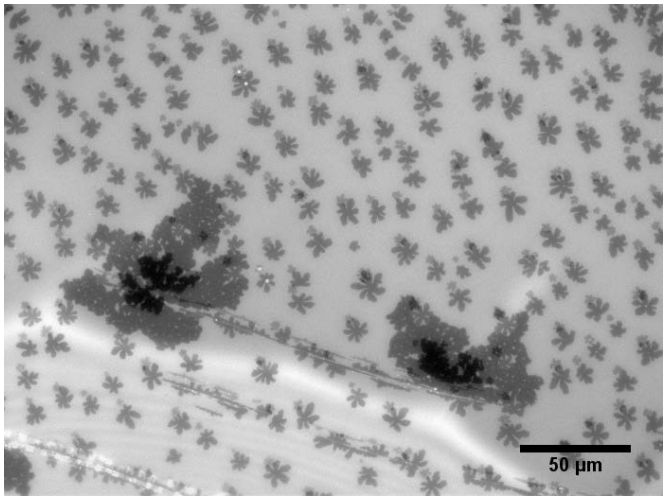

(c) 12a superpositioned on 12b.

Figur 12: The growth of $L_{\beta'}$ domains in an DOPC:DPPC (1:1 mixture) bilayer seen with the DiD probe and 20x magnification. Highlighted on 12b is: (A) a domain trapped inside a hole, (B) three domains screen of a smaller fourth domain, (C) an isolated domain which is very symmetric.

objective when they are a few micrometers in diameter. The domains are the dark grey blobs on the light gray background. The even lighter fringes at the bottom of the image is an optical artifact caused by a small pocket of air or water beneath the mica instead of the silicone glue which should be in contact with the entire mica surface. The large black objects are holes in the membrane where where no lipids are present.

On figure 12a the membrane is just below the $L_\alpha \rightarrow L_{\beta'}$ transition temperature which is $T_m \approx 34°C$ for DOPC:DPPC mixtures. At this point in time all nucleation sites are formed and we the growth of the domains is well under way. Upon closer examination rosette shapes can already be seen for some of the larger domains. Two large holes can be seen in the membrane. These from and

grow larger as the domains grow larger because the area per lipid becomes smaller when the lipids go from the l_α phase to the $L_{\beta'}$ phase. This causes stress to build up in the membrane and at some point this stress is relieved by the membrane contracting and forming holes. The holes often form around already existing holes in the membrane. Often holes are created during the rinsing procedure due to excessive rinsing. These holes then simply expand during the domain growth process.

Figure 12b shows the membrane after the cooling procedure has ended and the temperature has stabilized at $T = 20°C$. The domains have grown larger and still appear as rosettes. The holes in the membrane have also grown significantly in size to compensate for the stretching of the membrane caused by the growth of the domains. Upon closer inspection of the two large holes domains appear inside the holes on small patches of intact membrane still in the L_α phase.

A superposition of the two images are seen on figure 12c. Form this it is seen that the membrane have shifted slightly compared to the optics between the two images. This is understood as a combination of the membrane contracting during the domain growth and mechanical movement of sample as a whole. The sample is not fixed at the bottom of the Petri dish, it floats on a small cushion of water and vibrations in the setup (table, microscope etc.) can cause it to drift slightly. The latter of the two effects are believed to be the predominant. The shift appears to be in the same direction for all domains; towards the lower left corner of the images in this example. This indicates that the domains remain in fixed positions in the membrane; namely where they nucleated. This qualitative observation is in agreement with the findings in [22]; that the nucleation sites fixed and that if the membrane is heated and cooled again the new nucleation sites will largely coincide with the previous ones.

A correlation between the domain shapes figure 12a and 12b can also be seen. Those domains which in the beginning look very circular with symmetric, evenly spaced leafs appear to retain this symmetry as they grow. The same is seen for the more skewed and asymmetric domains. Some many-body effects can also be seen, e.g. (B) on 12b. Here three domains shield of a fourth domain located between them three. This fourth domain is considerably smaller than the other three and the three shielding domains are seen to grow outwards away from the fourth domain in the center. Again this qualitative observation is in aggrement with [22] where it is found that each domain is contained within a single Voronoi cell in a Voronoi diagram constructed from the nucleation centers. They conclude that the spacial distribution of the nucleation centers have a large impact on the sizes and shapes of the domains.

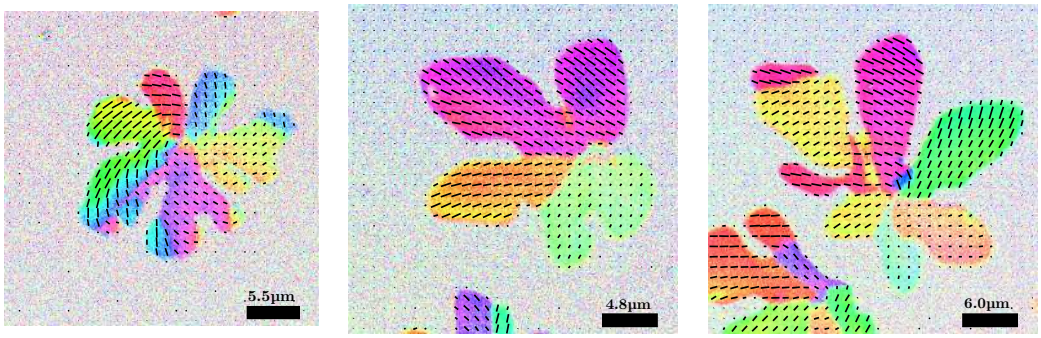

(a) (b) (c)

Figur 13: Texture of DOPC:DPPC (1:1) gel domains from three different samples.

3.2 Shape and texture of single domains after ended initial growth

The majority of the time spent in front of the microscope have been used to image single domains. An area of interest on the sample, like the area shown in figure 12, was found using the DiD probe and the camera. Then then using the laser scanning mode of the microscope every possible domain within the region was scanned one by one by choosing a scanning area just large enough to box the whole domain. This was done to maximize the resolution of the single domain and to reduce the time needed for scanning. The same resolution could have been achieved by scanning a larger area, but that would have taken longer time since large empty areas would also be scanned.

Figure 13 shows three DOPC:DPPC gel domains from three different samples all prepared with the same sample solution, i.e. the exact same lipid/probe composition. All of them show the vortex like change in angle director about their center. From [12, 20] the DOPC:DPPC mixture is expected to display a vortex texture between that of pure bend and pure splay and the textures obtained in this work agrees with this. The director angles neither points radially out from the center (splay) or is tangential to the center (bend). The three domains however display quite different spacial distribution of the director angles and quite different partitioning into subdomains with similar texture. Domain 13b and 13c are both partitioned into a number of subdomains all with their own local, uniform texture. Not much change in the director angle is seen within a single leaf or subdomain. Domain 13a on the other hand display a very noticeable change in director angle within each leaf and the partitioning into subdomains with uniform texture is not evident. The number of subdomains with uniform texture also vary from domain to domain. Domain 13b is partitioned into three subdomains with uniform texture whereas domain 13c is divided into six or seven subdomains with uniform texture, depending on how one counts. The all of the three areas colored red/purple have the same director angle, but they are separated in spatially with

no apparent reason for them to align with one another. This variation among domains in DOPC:DPPC bilayers from sample to sample, and even from one area of a sample to another, was observed repeatably throughout the experimental work.

A relevant question to ask is what causes this variation in the number subdomains with uniform texture and what causes some domains not to partition into such subdomains. The lipid composition does not change from sample to sample and the thermal history of the samples are the same from the time of rinsing and going forward. In [20, 22] it is speculated that the solid support substrate might play a role. Mica is a natural mineral and its surface, freshly cleaved or not, will vary from sample to sample. As discussed earlier the presence of salts the solution, used to hydrate the bilayers, decouples the bilayer sufficiently from substrate for the two leaflets to phase transition at the same temperature, compared to when no salts a present. So in some respect the bilayer and the substrate is less coupled than it could be, but even so they are still very much coupled. The bilayer interacts sufficiently with the substrate to not float away into the surrounding body of buffer solution. Supported bilayers also have their phase transition temperature shifted to a higher temperature compared to their unilamilar vesicle counterparts. In [22] a strong correlation between the position of nucleation sites for consecutive heating and cooling of a single membrane is found. They attribute this correlation to substrate. A possible test to confirm or rule out the substrate the inducer of these differences would be to repeatedly melt and grow domains in the same bilayer. This could reveal that the texture is identical for consecutive growth processes on the same bilayer, or it could reveal that they are uncorrelated. One could also systematically compare different regions of the same bilayer after a single growth procedure.

Many-body effects are also seen in 13c. The domain in the center has clearly grown in the direction away from the domain visible in the lower left corner. This seems to have caused two or three of the leafs to be substantially smaller than the others. The texture however does not seem to be particularly affected by it. The yellow subdomain pointing towards the other nearby domain is smaller than the others, but as clearly partitioned as the others and just as uniform in its director angles. Also there is no apparent coupling between the texture of the two domain even though they are in very close proximity of one another. Even though this is just an qualitative observation it could indicate a decoupling between the texture and the shape of the domain at this stage in the existence of the domains. This is also backed by comparing the physical shape of all three domains. All of them feature spatially separated leaf-like shapes. All of which have rounded smooth edges. Yet they display very different spatial distribution of director angles.

Another thing which is immediately visible from the three domains is the director angles correlation with the boundary/interface normal. On both figure 13b and 13c this is very easy to see from the large subdomains. If the boundary of

either domain is visually traced director angles will be seen to be orthogonal to the boundary in some places and parallel to the boundary in other places. This agrees with the findings in [12] where this is systematically investigated by constructing histograms of the angle between the director angle and the boundary/interface normal. These distributions are shown to be nearly uniform. This is a further indication of the decoupling of texture and shape.

All textures and shapes of domains shown thus far, and found in the literature ([11, 12, 22] to name a few), are from domains which have existed for anywhere between 10 minutes and 12 hours. During this period of time no apparent change in shape or texture is happening. Domains imaged after having existed for 20 minutes looks remarkably similar to domains imaged after several hours. This is however not the case if the domains are followed systematically for longer periods of time. This will be shown in the next section.

3.3 Time-resolved microscopy of gel domains

One of the first questions asked when someone sees the rosette shaped gel domains and their texture is if they are stable and in equilibrium. The question is to TODO(can I say "my"?) my knowledge not answered in the existing literature, especially not for extended periods of time. The initial aim of the long-term experiments presented in this section was simply to see if the texture of the domains remained stable for longer periods of time. The expected answer from existing short-term observations was that they were stable. Nothing had suggested otherwise form the single domain observations. However both the texture and the shape of the domains change dramatically over the course of days.

3.3.1 Shape and size

Figure 14 shows three frames from a 72 hour (20 minute resolution) image series of a DOPC:DPPC (1:1) bilayer kept at constant a constant $T = 20 \pm 0.5°C$. The three frames show that almost all domains change their shape and some even their center of mass. Three examples of behavior have been high lighted in the frames. The domain A, when followed through the frames is seen to be rounded off by shrinking. The leafs of the rosette is melted away. Domain C on the other hand is observed to rounded off of by growing. The fjords separating the leafs are filled out by lipids solidifying. The two domains marked as B are seen to be merging and form one larger domain. This is not done by translation of the entire domain, but rather by one domain growing and the other domain moving its center of mass by melting on one side and growing on another. This process of merging is a rare event compared to just growing or shrinking.

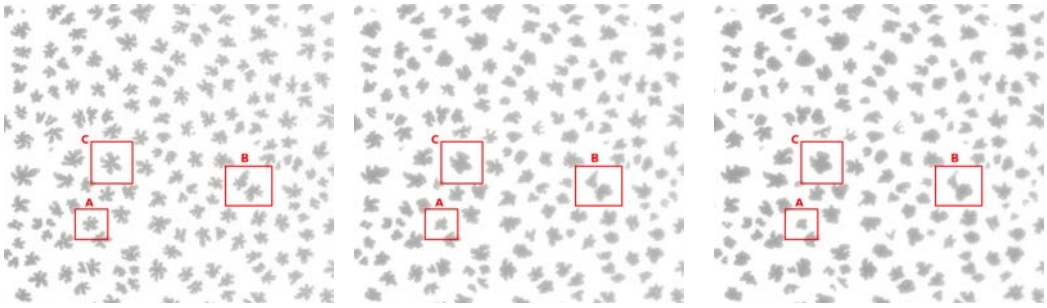

(a) $t = 0$ (b) $t = 39$ hours (c) $t = 78$ hours

Figur 14: Three frames a 78 hour image series of a DOPC:DPPC bilayer kept at constant temperature.

Figure 15 shows the area fraction $\frac{A_{gel}}{A_{liquid}}$ as a function of time and the sum of all domain perimeter lengths a function of time. The sum of all perimeter lengths is seen to decrease as would be expected since all the domains appear to become more circular as time passes. The area fraction is seen to remain almost constant $\frac{A_{gel}}{A_{liquid}} = 0.38 \pm 0.01$. This is obtained by thresholding the raw DiD wide field images to segment the gel domains from the liquid order background. Before thresholding the images were corrected differences in illumination. The area imaged is so large that the profile of the light source is visible in the raw images. Also over the course of 78 hours the output of the lamp varies slightly. Both these effects make it impossible to select a single meaningful threshold for all images. Correcting for the intensity of the lamp was simply done by normalizing the pixel intensities. Correcting for the illumination profile was done by fitting two second degree polynomials to the pixel intensities in horizontal and vertical direction. All pixels could then scaled by fitted polynomials such that dark pixels become brighter and vice versa. The frames shown in figure 14 are corrected in this manner. The two areas was then found simply by counting white and black pixels in the now binary image. The threshold value was chosen such that no two domains, known to be separate domains, would be detected as one, and such that no small domains were found to vanish due to the thresholding. The error estimates for both the perimeter length and the area fraction is estimated by a minimum and maximum threshold value fulfilling these two conditions.

The area fraction can be compared individual to the phase diagram for DOPC:DPPC to determine whether they are in thermodynamic equilibrium or not. Equation 2 and 1 can be modified to give the area fractions instead of the molar fractions. First the ratio between X_l and X_s is found:

$$\begin{aligned}\frac{X_{L_{\beta'}}}{X_{L_\alpha}} &= \frac{W_s - W_l}{W_s - X_{DPPC}} \cdot \frac{X_{DPPC} - W_l}{W_s - W_l} \\ &= \frac{X_{DPPC} - W_l}{W_s - X_{DPPC}}\end{aligned}$$

To get from the molar fraction of the two phases to the area fraction of the two phases the area per lipid of the constituent species are needed, for each phase. This is because both the $L_{\beta'}$ or L_α phase is comprised of both species. I have however in the literature been unable to find for area per lipid for both DOPC and DPPC in both phases. So instead the approximation that the area per lipid in each phase is the same as the area per lipid of the dominant species in that phase is used. This approximation have been used by [23] to compare area fractions of binary giant unilamilar vesicles to phase diagrams. The dominant species in the $L_{\beta'}$ phase is DPPC so $a_{L_{\beta'}} = a_{DPPC,L_{\beta'}} = 47.9\text{Å}^2$ and the dominant species in the L_α phase is DOPC so $a_{L_\alpha} = a_{DOPC,L_\alpha} = 72.5\text{Å}^2$ [24].

$$\frac{A_{L_{\beta'}}}{A_{L_\alpha}} = \frac{a_{L_{\beta'}}}{a_{L_\alpha}} \frac{X_{DPPC} - W_l}{W_s - X_{DPPC}} \tag{7}$$

W_s, w_l is read off the (original of the) phase diagram in figure 3 and found to be $W_s = 0.9 \pm 0.01$ and $W_l = 0.3 \pm 0.01$. $X_{DPPC} = 0.5$ for a 1:1 mixture of DOPC and DPPC. Plugging these numbers into eq. 7 gives:

$$\frac{A_{L_{\beta'}}}{A_{L_\alpha}} = 0.3$$

The uncertainty on this number is hard to estimate because the uncertainty of the area per lipid is unknown. Quite a few approximations lay behind those numbers and even if those approximations ignored the area per lipid values them selves vary substantially throughout the literature[24]. Also the phase diagram is for a supported bilayer system, but for multilamilar vesicles. All these uncertainties taken into account there seems to be agreement between the area fraction obtained from the DiD images and the one obtained from the phase diagram. A future study should try to determine the phase diagram for the supported bilayer system via for example atomic force microscopy for better comparison.

The perimeter length and area as a function of time for the individual domains have also been found and can be seen on figure 18. The area per domain as a function of time show three different behaviors consistent with the qualitative observations from figure 14. The area per domain have been normalized with respect to the initial area of each individual domain. From a $A_{domain} = 1.0$px the curves split into three groups: some areas which grow, some areas which shrink and some areas which remain more of less constant compared to the other two groups. So the area fraction is kept constant by having some domains shrink and some domains grow, precisely as seen in the three frames. From the individual perimeter length curves it is seen that the total decrease in perimeter comes from all domains decreasing their perimeter. This confirms that all domains tend to be rounded off as time goes by, but they do it via different methods. Some have their perimeter costly features melted away, some fill out the perimeter costly fjords with additional solidified lipids and finally some do both.

This is not classical coarsening sine the domains them selves stay in fixed positions. Somehow they still exchange material with each other or the surrounding

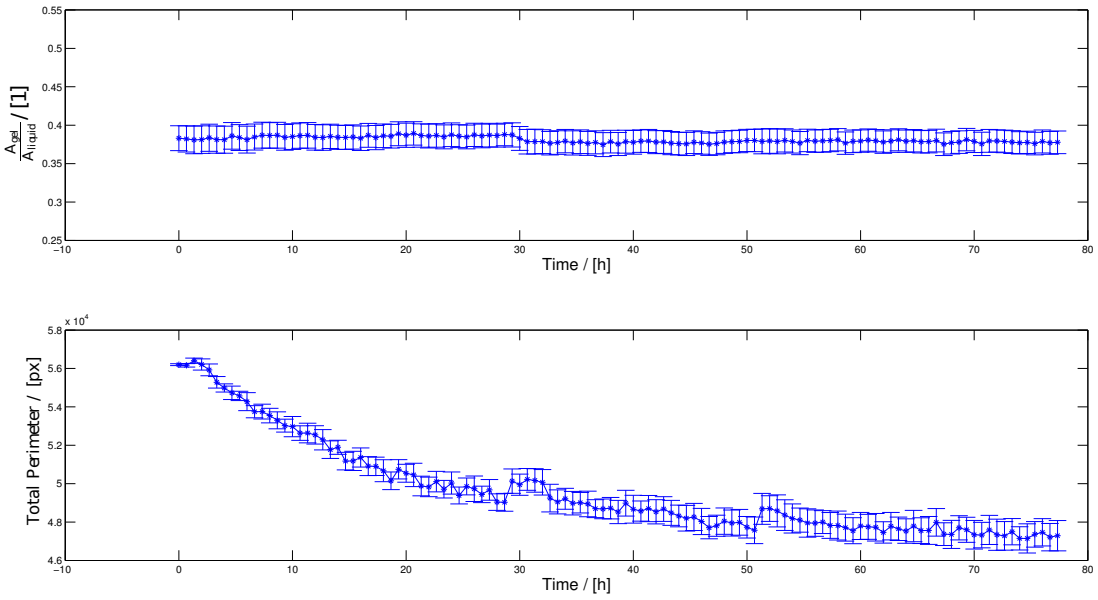

Figur 15: The ratio between area of the gel phase and area of the liquid phase, and the total perimeter of all domains as a function of time.

fluid phase which is a reservoir of both species. To try to confirm, or rule out, the model of them exchanging material with other nearby domains the correlation function between growth rate and distance have been calculated. Figure 17 shows the binning of the domains by distance to a given test domain. The total growth rate for each bin is calculated as the sum of the individual growth rates in that bin:

$$\frac{dA_k}{dt} = \sum_{i \in k} \frac{da_i}{dt} \tag{8}$$

where k enumerates the bins and $\frac{da_i}{dt}$ for $i \in k$ is the growth rate of the i'th domain within bin k. The correlation function $C(r)$ is then given by:

$$C(r) = \frac{(\frac{dA_k}{dt} - \mu)(\frac{dA_{k+r}}{dt} - \mu)}{\sigma^2} \tag{9}$$

where r is the distance between bins measured units of bins. This correlation function can be computed with each domain as the test domain to improve the statistics. Negative correlation will mean that a decrease in area somewhere is compensated by an increase in area elsewhere and a positive correlation will mean that an area increase (or decrease) somewhere is matched by an area increase elsewhere. If the domains exchange lipids with nearby domains we should see a large negative correlation for short distances, meaning that the growth of the test domain is compensated by negative growth nearby (and vice versa). Figure 16 shows the correlation function. Even when averaged over all the correlation functions computed for each domain it shows no apparent features besides noise. This could indicate that the domains do not exchange lipids with each other, but rather just shed lipids to or recruit lipids from the surrounding liquid phase.

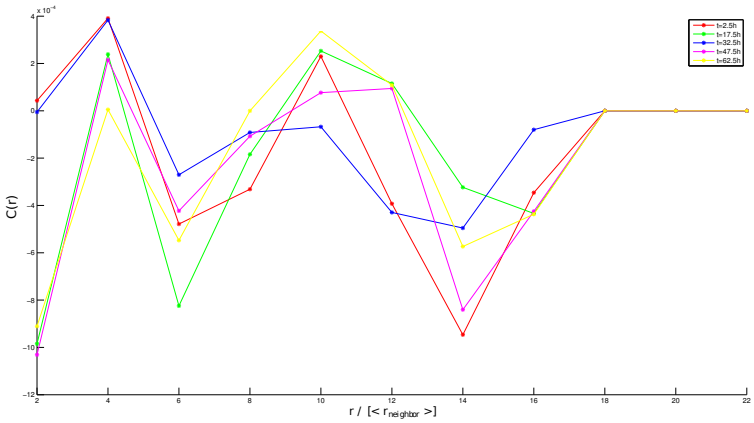

Figur 16: The domains binned by distance to a test domain. The test-domain is the domain without number and center for the concentric circles that visualize the bins.

The last the thing investigated from these time lapse images is whether the sign of the growth rate $\frac{da}{dt}$ is dictated by the size of the domains, i.e. is it domains below a certain size that shrinks and domains above a certain size that grows. Figure 19 shows the distribution of domain area size for domains growing and shrinking. From the histograms it is seen that shrinking or growing does not depend on the size of the domain. Domains of all sizes are seen to both grow and shrink.

3.3.2 Texture

The texture of all domains in an large area of a DOPC:DPPC bilayer was imaged over a period of 7 days, once per day. This temporal images sequence is seen in figure 20. It is seen that the texture changes together with the shape of the domains. The number of leafs or subdomains for each domain seems to be the same throughout the 7 day observation window. They do however change in size relative to one another. Some subdomains shrink while others grow. At $t = 7$days most domains are seen to have 1-2 subdomains which have been considerably enlarged compared to $t = 0$. The texture within the subdomains that grow or shrink change a little, but each subdomain maintains its own unique director orientation compared to the other leaflets. The overall texture of the domains tend towards larger areas of uniform texture. From this 7 day observation it cannot be discerned what the configuration is at $t = \infty$.

Figure 21 show two DOPC:DPPC domains after they have relaxed for two months in the laboratory. All this time they have not been situated on the microscope, but stored in the dark a room with temperature control. Their precise thermal history throughout this month is not known however. They have been in

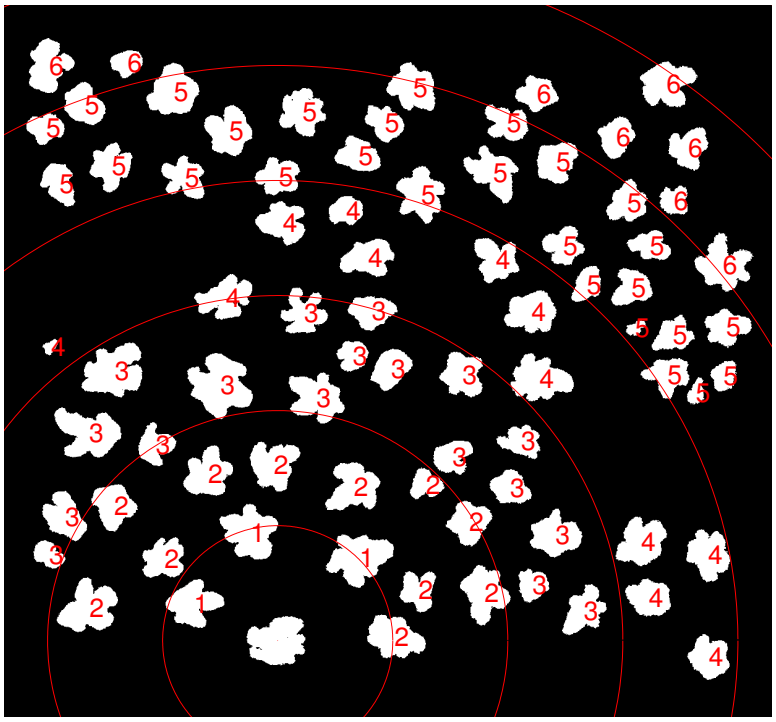

Figur 17: The domains binned by distance to a test domain. The test-domain is the domain without number and center for the concentric circles that visualize the bins.

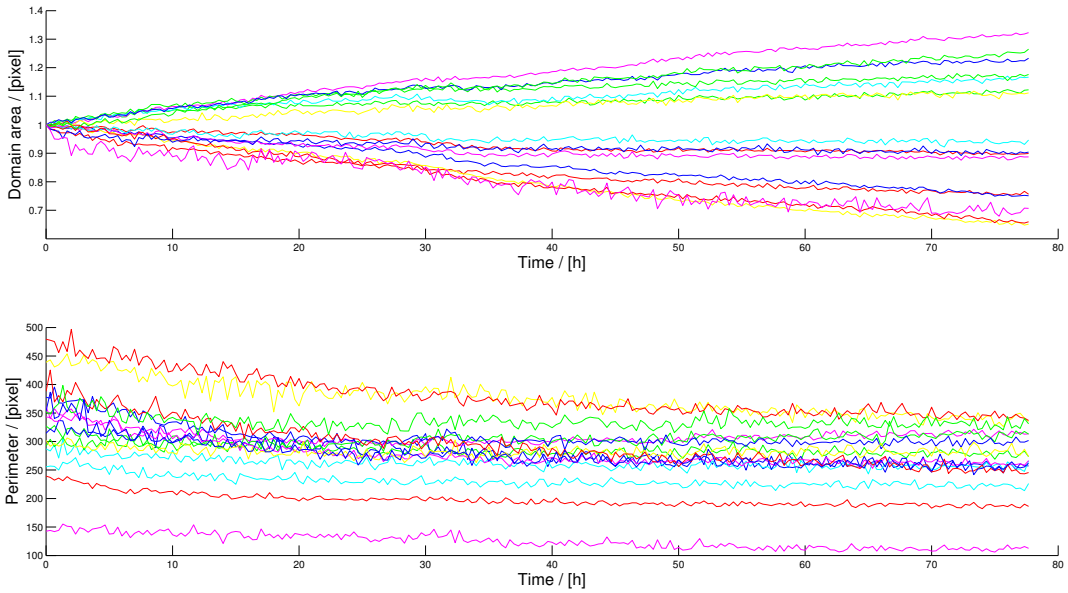

Figur 18: The correlation function $C(r)$ at different times throughout the image series.

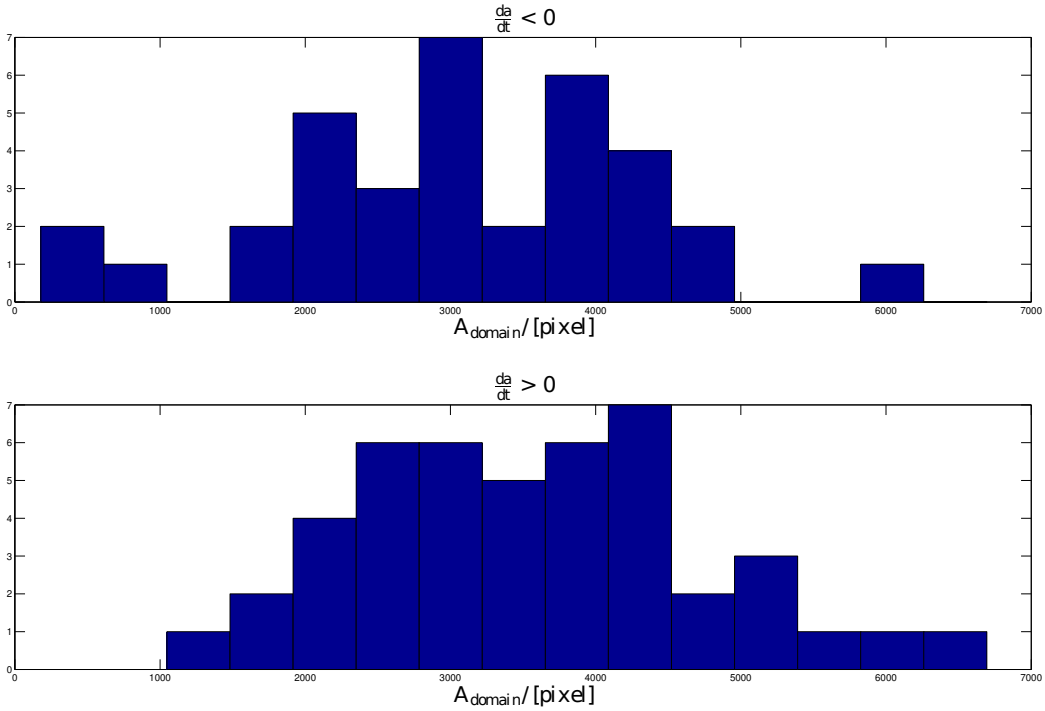

Figur 19: Two histograms showing the distribution of area size for domains growing and shrinking respectively.

thermal equilibrium with the room they were located, which were air conditioned to be $\sim 22°C$ which is very close to the temperature the membranes are kept at during imaging. They are seen to have continued the tendencies found during the 7 day experiment. They have become even more rounded of and the fraction of the domain covered by a single uniform texture has increased substantially. The left-most domain almost only have two orientations left. The defect which to begin with was situated in the center of the domain is now located at the edge of the domain. Based on the observations from the DiD time lapse and the 7 day texture time lapse the defect has remained stationary relative to the membrane and the domain have moved around it. Melting on one side and growing on the other.

3.4 Summary of experimental results

This section is a short summary of what have been found experimentally and concluded in the previous experimental sections.

- The gel domains are observed experimentally to have two stages of growth at vastly different time scales.

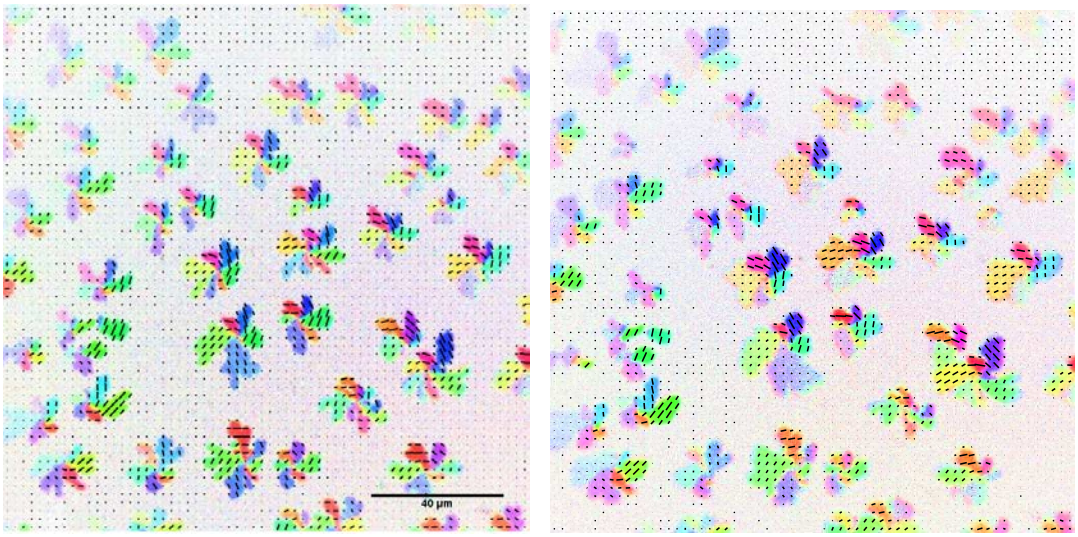

(a) $t = 0$ (b) $t = 3$ days

(c) $t = 5$ days (d) $t = 7$ days

Figur 20: The texture of domains in a large area of a sample.

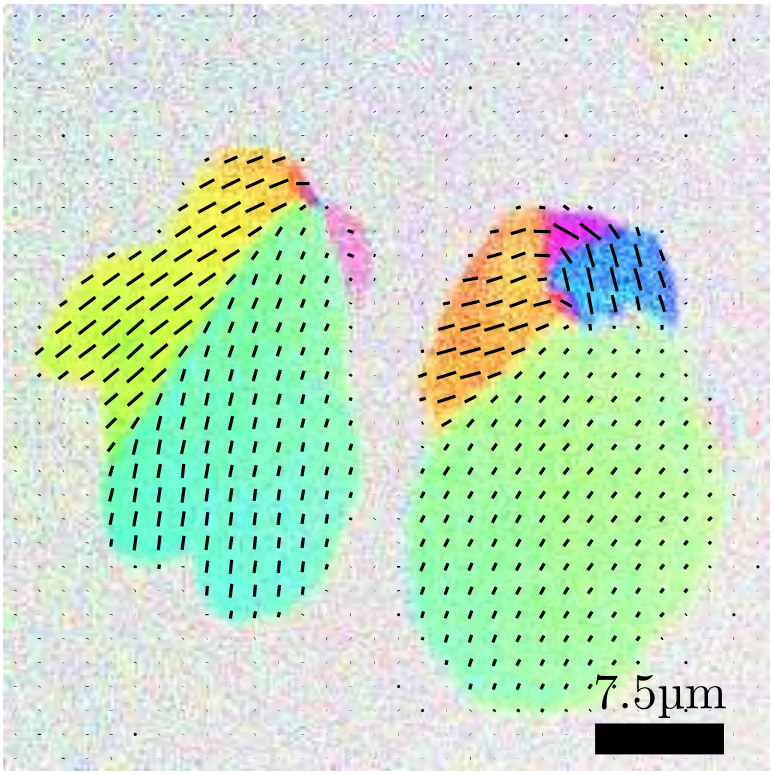

Figur 21: The texture of two DOPC:DPPC after one month of relaxation.

  - On the timescale associated with the cooling of the sample from $T = 60°C$ to $T = 20°C$ they grow subject to rules which cause them to become rosette shaped.
  - On much longer timescales these rules play little role and the domains relax into more circular shapes; either by growing larger or by melting to shed the rosette features.

- Many-body effects are observed to play a significant role in the shape of the domains. Some domains are shielded of by other domains and cannot recruit as many lipids to grow from as more isolated domains. This cause the domains to become skewed and asymmetric.

- No evidence is seen to suggest a coupling between the texture and the shape of the domain at short timescales. A coupling at longer timescales is possible.

- The texture of the domains is seen to tend towards fewer, larger subdomains with uniform texture.

- The domains are immobile except for their ability to melt on one side and grow on another.

These observations are the input used to construct diffusive model of gel domains in the next section.

4 A Diffusion Limited Aggregation model

In this section a diffusion limited aggretation model for the domain growth is motivated, qualitatively convincing results presented and future work outlined.

4.1 Motivation

When one constituent of a binary mixture begins to transition from a liquid phase to a solid phase spatial transportation of the two constituents need to take place. The area surrounding nucleation sites have the wrong composition of the constituents compared to what it will be when the phase transition is complete. Take as an example the nucleation and solidification of DPPC in the DOPC:DPPC binary mixture. At time of nucleation the area surrounding the nucleation site is a 1:1 mixture of the two species. After ended initial growth it is a 1:9 composition (DOPC:DPPC) which make up the gel domain. This mean DOPC have to be transported away from the nucleation site and DPPC have to be transported to the nucleation site. The method of transportation available to the lipids in the membrane is lateral diffusion. If the growth rate is sufficiently large the limiting factor will be the mass transfer by diffusion. Such diffusion limited growth is known to create fractal, loosely packed structures where growth is happening only at outermost edges of the structure. A successful model for such growth is called diffusion limited aggregation (DLA) and was first proposed in 1981 by physicists T. A. Witten and L. M. Sander[25].

Since the domains, or DPPC aggregate, is observed to grow structures which have some of the same characteristics as DLA clusters and since diffusion is known to be the only mode of transportation for the lipids a DLA model is an obvious first guess for a model of the domain growth. This thesis is not the first to make these observations. In [22] it is remarked that the rosette shapes of the domains is likely an indicator of the growth being limited by diffusion. Several features are however quite different from the original DLA model purposed by Witten and Sander. The domains are observed to be much closer packed than a classical DLA aggregate and they do not only have a shape, they also have orientational texture and they are not symmetrical like classic DLA aggregates.

Modifications to the DLA mhooseodel have been proposed which will course closer packing of the aggregate. They first and foremost include the addition of line tension and local surface relaxation[26]. Since the binary lipid system is

known to have a line tension between its two phases due to hydrophobic mismatch such an modification is easily justified.

4.1.1 The DLA model

The DLA model proposed for the domain growth is a classic DLA model modified by adding line-tension and local surface relaxation. The texture is modeled by assigning each particle of the DLA cluster an angle which can vary between $[0, 2\pi]$, an analog to the director angle from the experimental textures. Since it is not known why the domains have a central defect and it is not easily discerned experimentally this model focuses on the growth after the formation of the central defect. The growth model, or algorithm, is as follows:

1. A small seed cluster (10-100 DLA-particles) is placed in a coordinate system. The particles making op the seed is assigned angles which mimic the angle field created by the two central $+\frac{1}{2}$ defects observed experimentally.
2. A new particle, called the walker, is placed in the same coordinate system as the seed, but far away from the seed.
3. The walker makes a random walk until it comes into contact with the seed.
4. When it comes into contact with the seed (or existing aggregate) it has a probability for aggregating which depends on the curvature of the a seed (or aggregate) in such away that the probability for aggregating a convex regions is less than that for aggregating at concave regions. If the particle aggregates the algorithm goes back to step 2. If the particle does not aggregate the algorithm goes back to step 3.
5. When the particle has aggregated is allowed to move along the perimeter to minimize its energy with respect to the surface tension. I.e. it is allowed a fixed number of Monte-Carlo sweeps to try and find a position with lower energy. When all sweeps are completed the particle is aggregated.
6. After the particle have aggregated it is assigned a director angle φ_c which is the mean director angle of the particles neighboring the newly added particle. This angle is also relaxed using a fixed number of Monte-Carlo-sweep where the energy is the classical XY-model configuration energy.
7. Go back to step 2.

As seen from the description of the modified DLA algorithm there is no coupling between the texture and the shape of the cluster. This was chosen because no such coupling is evident from experiments. The shape of the domain is governed entirely by the modified DLA-mechanics and then texture entirely the the

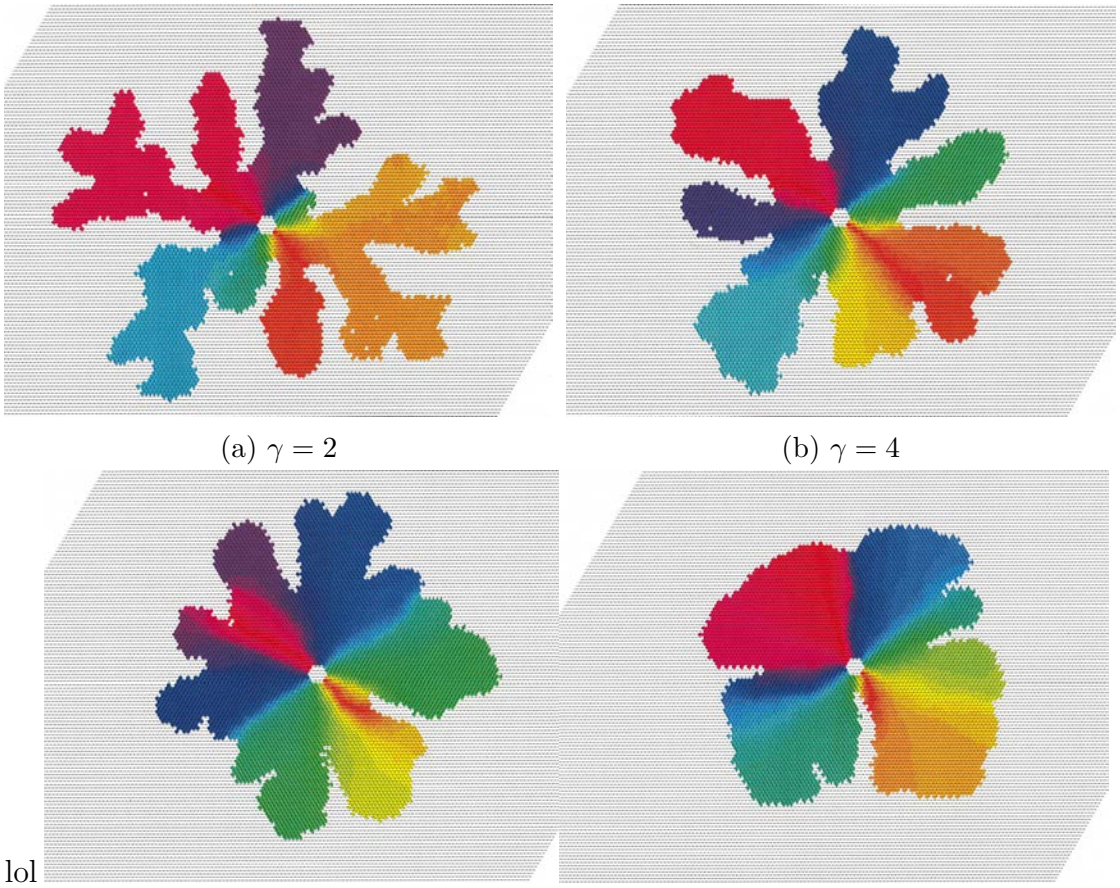

(a) $\gamma = 2$ (b) $\gamma = 4$

lol

(c) $\gamma = 6$ (d) $\gamma = 8$

Figur 22: Four clusters grown by the modified DLA algorithm with four different line tensions. The hole in the center is where the vortex seed is located.

the new particle aligning it self with its local neighborhood. The algorithm was developed in collaboration with fellow student Glenn G. B. Nielsen and the initial implementation of the algorithm on a hexagonal grid was written by Glenn. Without further discussion of the algorithm four clusters grown by the algorithm is presented on figure 22.

To the naked eye the four clusters looked remarkably similar to the experimentally grown domains. Some of them more than others. For the lowest value of the line tension $\gamma = 2$ the cluster is too open and loosely packed. For the highest value of the line tension $\gamma = 8$ the cluster is too closely packed to resemble the early stages of the experimentally grown domains. For $\gamma = 4$ the resembles is very convincing to the eye.

Lots of other parameters than γ can be tuned. The number of sweeps used to relax the perimeter and director angles, the temperature which is part of the acceptance probability of the Monte Carlo sweeps etc.

When structures first appeared from the simulations the focus shifted from refining the simulations to comparing the simulations to experimental data. The comparisons suggested at the time were all statistical: total director angle distribution, director angle distributions within subdomains, number of subdomains, area to perimeter ratios etc. At the time the simulation produced these structures only a very limited experimental data set existed from the work of Jes Drier[12]. Jes' focus had been on many different phenomenon related to texture and with many different lipid mixtures and compositions. So no large set of images of a single type of domain was made. This caused the focus to shift from comparison to experimental data, to obtaining experimental data. By the time the experiments were producing data which could be used for comparison to the simulations long-term behavior and lack of stability of the domains were discovered. This caused yet another shift in focus towards observing these stages of the domain existence experimentally and how the simulations could be modified to account for these new phenomenons. The simulation on the hexagonal grid was left as a proof of concept and focus shifted towards implementing an off-lattice simulation which could account for long-term behavior of domains. The decision to implement an off-lattice version was made to eliminate effects of the underlying grid of the lattice model. Finding hexatic order on a hexagonal grid might be an artifact of the grid. Particularly the long-term relaxation effects would be vulnerable to grid-artifacts since we have already seen that with high enough line tension (γ) the structure grown is not a circle but a hexagon.

Considerable time and resources was spent on reimplementing the algorithm off-lattice and extending it to allow the domains to stop growing and reorganize. As the ambitions were soaring on behalf of the algorithm it was decided also to include many-body effects in the off-lattice algorithm by allowed multiple clusters to coexist and compete for walkers on the same lattice. The off-lattice simulation is therefor still in the making. At moment of writing it can produce compact clusters with textures similar to those seen in the lattice DLA-model, and it can display some of the many-body effects observed experimentally, for example the skewing and screening of domains by other domains. Figure 23 shows one of the early many-cluster simulations without texture and close-packing. The DLA clussters can be seen to exhibit asymmetrical growth and some clusters are much smaller than other clusters due to screening effects. The off-lattice models as it is now is a good base for further development. Much time have been invested in designing and choosing data structures to ensure it performs well[27, 28] and is easy to extend with new features. The simulation shown on figure 23 with $\sim 10^6$ particles were completed in less than a minute on a normal laptop using less than 2GB of memory. The normal data structures and decision flows for on- and off-lattice DLA are not designed to handle many clusters growing at the same time, clusters merging and the growth stopping and the structures relaxing their shape by letting particles detach from the clusters again.

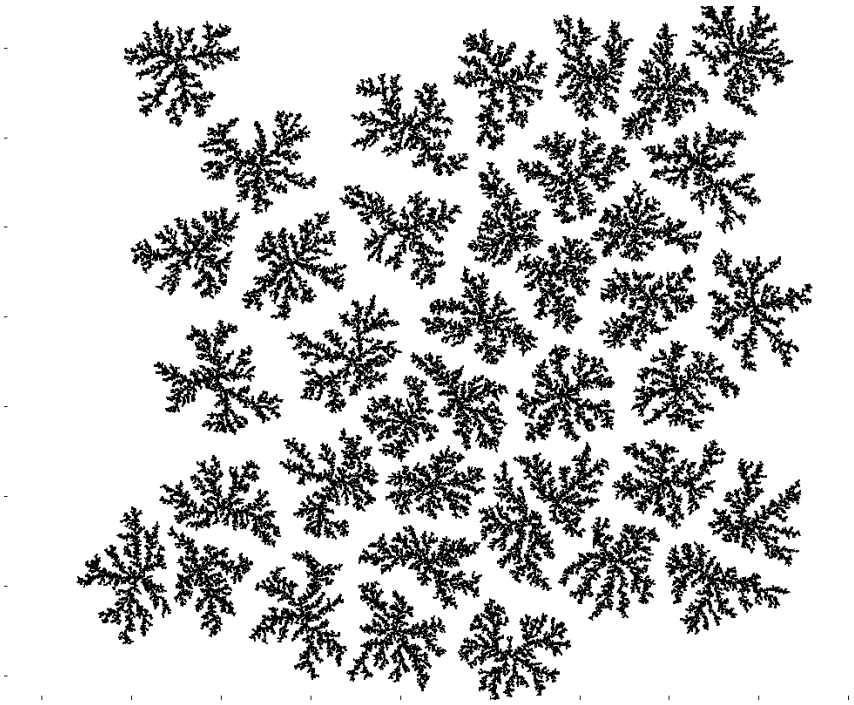

Figur 23: Off-lattice simulation of 30-40 clusters competing for $\sim 10^6$ particles.

4.1.2 Taking the simulations further

This project leaves a lot of work yet to be done. A number of interesting questions remains unanswered and this section gives a short description of what can be done in future work.

The first question that remains to be answered is whether the DLA-like model can be shaped to reproduce the long-term behavior of the domains. If a stop in growth is implemented and the particles allowed to detach from the clusters and reattach themselves elsewhere, will this give time-lapse sequences like the once seen experimentally where some domains grow and some shrink? Will The drop perimeter and areas as a function of time look like those seen experimentally?

Another interesting question is what happens if a coupling between the texture and the shape is made? Will we see the domains tending towards uniform texture like seen experimentally? Will they melt and grow to exclude the nucleation defect like seen experimentally? Will they show this behavior without an coupling between texture and shape?

Litteratur

[1] P. W. Atkins. *Physical Chemistry*. Oxford University Press, 1998.

[2] Mats Hillert. *Phase Equilibria, Phase Diagrams and Phase Transformations: Their Thermodynamic Basis*. Cambridge University Press, 1998.

[3] Uffe Bernchou, Henrik Midtiby, John Hjort Ipsen, and Adam Cohen Simonsen. Correlation between the ripple phase and stripe domains in membranes. *B B A - Biomembranes*, 1808:2849âĂŞ2858, 2011.

[4] K. Furuya and T. Mitsui. Phase Transitions in Bilayer Membranes of Dioleoyl-Phosphatidylcholine/Dipalmitoyl-Phosphatidylcholine. *Journal of the Physical Society of Japan*, 46:611, February 1979.

[5] D. Keller, N.B. Larsen, I.M. MÃÿller, and O.G. Mouritsen. Decoupled phase transitions and grain-boundary melting in supported phospholipid bilayers. *Physical Review Letters*, 94(2):025701, 2005.

[6] Anne Feng Xie, Ryo Yamada, Andrew A. Gewirth, and Steve Granick. Materials science of the gel to fluid phase transition in a supported phospholipid bilayer. *Phys. Rev. Lett.*, 89:246103, Nov 2002.

[7] Siewert J. Marrink, Jelger Risselada, and Alan E. Mark. Simulation of gel phase formation and melting in lipid bilayers using a coarse grained model. *Chemistry and Physics of Lipids*, 135(2):223 – 244, 2005.

[8] Kasper RÃÿrdam Jensen. Growth of gel-domains in lipid bilayers: Dependence of the nucleation process on cooling rate and lipid composition. Supervisor Adam C. simonsen and John H. Ipsen.

[9] A A Brian and H M McConnell. Allogeneic stimulation of cytotoxic t cells by supported planar membranes. *Proceedings of the National Academy of Sciences*, 81(19):6159–6163, 1984.

[10] Ulrike Mennicke and Tim Salditt. Preparation of solid-supported lipid bilayers by spin-coating. *Langmuir*, 18(21):8172–8177, 2002.

[11] Adam Cohen Simonsen and Luis A. Bagatolli. Structure of spin-coated lipid films and domain formation in supported membranes formed by hydration. *Langmuir*, 20(22):9720–9728, 2004. PMID: 15491207.

[12] Jes Dreier. *Orientational Texture of Lipid Bilayer and Monolayer Domains*. PhD thesis, University of Southern Denmark, 2012.

[13] Douglas B. Murphy and Michael W. Davidson. *Fundamentals of Light Microscopy and Electronic Imaging*. Wiley-Blackwell, 2012.

[14] Inc Molecular Probes. Certificate of analysis for 6-dodecanoyl-2-dimethylaminonaphthalene (laurdan). Technical report, Molecular Probes, Inc, 2012.

[15] T. Parasassi, G. De Stasio, A. Dubaldo, and E. Gratton. Phase fluctuation in phospholipid-membranes revealed by laurdan fluorescence. *Biophysical Journal*, 57:1179–1186, 1990.

[16] L. Bagatolli, E. Gratton, T.K. Khan, and P.L.G. Chong. Two-photon fluorescence microscopy studies of bipolar tetraether giant liposomes from thermoacidophilic archaebacteria sulfolobus acidocaldarius. *Biophysical Journal*, 79:416–425, 2000.

[17] T. Parasassi, E. Gratton, W.M. Yu, P. Wilson, and M. Levi. Two-photon fluorescence microscopy of laurdan generalized polarization domains in model and natural membranes. *Biophysical Journal*, 72:2413–2429, 1997.

[18] Juhasz J, Davis JH, and Sharom FJ. Fluorescent probe partitioning in giant unilamellar vesicles of 'lipid raft' mixtures. *Biochem J.*, 430, 2010.

[19] Inc Molecular Probes. Certificate of analysis for 1,1'-dioctadecyl-3,3,3',3'-tetramethylindodicarbocyanine. Technical report, Molecular Probes, Inc, 2013.

[20] Jes Dreier, Jonathan Brewer, and Adam Cohen Simonsen. Texture defects in lipid membrane domains. *Soft Matter*, 8(18):4894–4904, 2012.

[21] Arthur Edelstein, Nenad Amodaj, Karl Hoover, Ron Vale, and Nico Stuurman. *Computer Control of Microscopes Using μManager*. John Wiley & Sons, Inc., 2010.

[22] Uffe Bernchou, John Hjort Ipsen, and Adam Cohen Simonsen. Growth of solid domains in model membranes: Quantitative image analysis reveals a strong correlation between domain shape and spatial position. *J. Phys. Chem. B*, 113(20):7170–7177, 2009.

[23] M. Fidorra, A. Garcia, J.H. Ipsen, S. HÃďrtel, and L.A. Bagatolli. Lipid domains in giant unilamellar vesicles and their correspondence with equilibrium thermodynamic phases: A quantitative fluorescence microscopy imaging approach. *Biochimica et Biophysica Acta (BBA) - Biomembranes*, 1788(10):2142 – 2149, 2009. <ce:title>Includes Special Section: Cardiolipin</ce:title>.

[24] John F. Nagle and Stephanie Tristram-Nagle. Structure of lipid bilayers. *Biochimica et Biophysica Acta (BBA) - Reviews on Biomembranes*, 1469(3):159 – 195, 2000.

[25] T. A. Witten and L. M. Sander. Diffusion-limited aggregation, a kinetic critical phenomenon. *Phys. Rev. Lett.*, 47:1400–1403, Nov 1981.

[26] R. Tao, M. A. Novotny, and K. Kaski. Diffusion-limited aggregation with surface tension. *Phys. Rev. A*, 38:1019–1026, Jul 1988.

[27] A. S. G., F. S. C., and M. M. L. Brazilian journal of physics. *Brazilian Journal of Physics*, 38:81–86, 2008. We review some computer algorithms for the simulation of off-lattice clusters grown from a seed, with emphasis on the diffusion-limited aggregation, ballistic aggregation and Eden models. Only those methods which can be immediately extended to distinct off-lattice aggregation processes are discussed. The computer efficiencies of the distinct algorithms are compared.

[28] F.L. Braga and M.S. Ribeiro. Diffusion limited aggregation: Algorithm optimization revisited. *Computer Physics Communications*, 182(8):1602 – 1605, 2011.